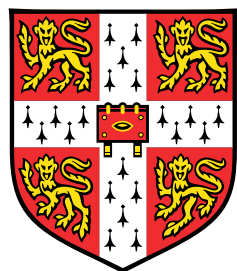


# Using 3D image data to improve 2D Brightfield image segmentation

## A method of 3D projection



**Nicholas Piano**

Department of Engineering  
University of Cambridge

This dissertation is submitted for the degree of  
*Master of Philosophy*

St Edmund's College

January 2016



I would like to dedicate this thesis to my long-suffering supervisor, Y. Y. "Shery" Huang, for her help and advice. Without her guidance, this would not have been possible.



## **Declaration**

I hereby declare that except where specific reference is made to the work of others, the contents of this dissertation are original and have not been submitted in whole or in part for consideration for any other degree or qualification in this, or any other university. This dissertation is my own work and contains nothing which is the outcome of work done in collaboration with others, except as specified in the text and Acknowledgements. This dissertation contains fewer than 15,000 words including appendices, bibliography, footnotes, tables and equations and has fewer than 150 figures.

Nicholas Piano  
January 2016



## **Acknowledgements**

And I would like to acknowledge the support and patience of my parents, my colleague Cristina Bertulli, and Xiaohao Cai.



## **Abstract**



# Table of contents

<b>List of figures</b>	xiii
<b>1 Introduction</b>	<b>1</b>
1.1 Segmentation in cell biology . . . . .	1
1.2 Current work in context . . . . .	2
1.3 Thesis outline . . . . .	3
<b>2 Imaging focus: the microfluidics environment</b>	<b>5</b>
2.1 Purpose and the need for segmentation . . . . .	5
2.2 Confocal microscope and 3D structure . . . . .	6
2.3 Description of the environment . . . . .	6
2.4 Live cell imaging limitations . . . . .	8
2.5 Autofocus and focal fluctuations . . . . .	9
<b>3 Background</b>	<b>11</b>
3.1 Introduction . . . . .	11
3.2 Cell microscopy, optical structure, and GFP distributions . . . . .	11
3.3 Image processing and segmentation . . . . .	12
3.4 CellProfiler and segmentation software . . . . .	17
3.5 Cell tracking . . . . .	20
3.6 The Selinummi brightfield profile method . . . . .	21
<b>4 Methodology</b>	<b>25</b>
4.1 Introduction to the method . . . . .	25
4.2 The GFP profile . . . . .	26
4.3 Optimum features for cell recognition . . . . .	28
4.4 zMod and zBF . . . . .	29
4.5 Artificial edges for segmentation: zVar and zEdge . . . . .	29
4.6 Protrusion measurement . . . . .	32

4.7 Summary of the method . . . . .	33
<b>5 Image processing results and discussion</b>	<b>37</b>
5.1 Introduction . . . . .	37
5.2 Parameter sensitivity study: $R$ , $\Delta Z$ , $\Sigma$ . . . . .	38
5.2.1 The radius of GFP linear smoothing: $R$ . . . . .	39
5.2.2 The brightfield level correction: $\Delta Z$ . . . . .	39
5.2.3 The radius of level Gaussian blur: $\Sigma$ . . . . .	41
5.2.4 Final choice of parameters . . . . .	41
5.2.5 The subject of the background . . . . .	42
5.2.6 Subsequent effects on zUnique and zEdge . . . . .	42
5.3 zVar and zEdge . . . . .	42
5.4 Comparison with common methods . . . . .	43
5.5 Errors and limitations . . . . .	44
<b>6 Conclusion</b>	<b>53</b>
6.1 Summary . . . . .	53
6.2 Further work . . . . .	54
6.2.1 Enhanced microscope imaging with live cell tracking . . . . .	54
6.2.2 Pre-processing to segmentation . . . . .	54
6.2.3 Cell dynamic modelling . . . . .	55
<b>References</b>	<b>57</b>

# List of figures

2.1	Sample image data . . . . .	7
2.2	Microfluidics device and data in context . . . . .	8
3.1	Possible GFP distributions . . . . .	13
3.2	Example of the Canny edge filter . . . . .	14
3.3	Sample of blob detection . . . . .	15
3.4	Watershed example . . . . .	16
3.5	Object masks . . . . .	17
3.6	Secondary object error example . . . . .	18
3.7	The LASSO tool . . . . .	19
3.8	Cell protrusion example . . . . .	20
3.9	Selinummi brightfield profile . . . . .	22
4.1	The GFP profile . . . . .	27
4.2	GFP scatter plot . . . . .	28
4.3	zMod example . . . . .	30
4.4	zBF example . . . . .	30
4.5	zVar example . . . . .	31
4.6	zUnique example . . . . .	32
4.7	zEdge example . . . . .	33
4.8	Protrusion calulation . . . . .	34
4.9	Method flow chart . . . . .	35
5.1	zBF comparison with brightfield . . . . .	38
5.2	Varying R . . . . .	40
5.3	Varying $\Delta Z$ . . . . .	40
5.4	Varying $\Sigma$ . . . . .	41
5.5	False Z variation . . . . .	43
5.6	Edges in low GFP regions . . . . .	44

5.7	Ineffective zEdge . . . . .	44
5.8	Testing: segmentation area comparison . . . . .	45
5.9	Testing: segmentation area comparison values . . . . .	46
5.10	Testing: protrusion comparison . . . . .	47
5.11	Unaccounted for: superimposed cells . . . . .	48
5.12	Effects of low GFP illumination . . . . .	49
5.13	Cross-level artefacts . . . . .	50
5.14	Lack of brightfield contrast . . . . .	51

# **Chapter 1**

## **Introduction**

### **1.1 Segmentation in cell biology**

An important part of live cell image analysis is the accurate measurement and tracking of cell morphology during an experiment. Using a microscope, there are many different ways of observing the cells ranging from brightfield microscopy to 3D fluorescence reconstructions. Both 2D and 3D shape data from the cells along with their speed and directionality can provide information on the effectiveness of drugs or other agents in the experiment. The processing of cell data often relies on the quality of Cell Segmentation, or the automatic or manual differentiation of Objects of Interest, such as cells, from the background. Many algorithms and software packages, such as CellProfiler and ImageJ, are used to segment cells automatically, yielding variable quality.

A key limitation in widely used software that this paper seeks to address is the inability to account for consistent features that cannot be easily located in 3D data. 3D image data, such as from a confocal microscope, contains information about an environment on many focal planes [2]. Objects can appear blurred or in focus depending the current focal plane. Consequently, features that are useful for segmentation; dark edges, uniform bright interiors, and other features such as fluorescent markers placed within cells are subject to any fluctuations in focus or the movement of objects vertically in the environment. This prevents consistent segmentation of the cell.

The environment used in this study is a microfluidics chip built to simulate a human blood vessel. This type of chip, a microchannel framework printed on a PDMS substrate, is seen as a potential revolutionary tool for future drug testing and development [16]. The 3D nature of this setup requires the use of confocal microscopy or similar methods to observe objects in all parts of the environment. In this case, a confocal microscope was used to record data in both a brightfield channel and a fluorescent GFP channel. The purpose of the GFP is described

more fully in Chapter 3.2. A number of limitations on the image quality, discussed in Chapter 2.4, prevent more powerful direct 3D methods to be used for segmentation. This necessitates a deeper investigation into how the currently available brightfield and GFP information can be used to segment the cells consistently.

## 1.2 Current work in context

The problem of consistently recognizing objects in a 3D environment using the brightfield is partially addressed in the 2009 study by Selinummi et al. [12] They attempted to remove the problem of finding objects in 3D by studying the variance of vertical brightness profiles in the brightfield. This had the effect of simplifying 3D data into a 2D plane containing relevant object shapes, from which segmentation could be done more easily. Although this was effective in their case, it has several disadvantages that the current work aims to solve. Notably, it performs poorly in a multicellular environment, necessary for this and many other studies. This is discussed in more detail in the method in Chapter 3.6.

The current work builds on the idea of studying vertical intensity profiles by applying this concept instead to the GFP. In the current data, the low quality GFP does not show the outlines of cells accurately. This is due to the internal cellular distribution of the GFP, described in Chapter 5. The central regions of the cell (not including the nucleus) are highlighted, so it can be used to locate the general bulk of the cell. The brightfield, on the other hand, shows the edges of the cell more clearly, but only if the cell is in focus (at the correct level). Edges of the cell start to fade along protrusions. In this study, any useful segmentation done must include accurate outlines of long cell protrusions to determine cell motility and behaviour.

The method described here uses the bulk of the cell visible in the GFP to locate the level in the data needed to ensure consistently clear dark edges in the brightfield, yielding accurate cell shape. The GFP and brightfield data represent the same physical space. This correspondence is exploited to allow information about the GFP channel to aid searching for features in the brightfield. The correct edges are located by building a vertical GFP intensity distribution for each pixel and selecting pixels from the brightfield data that match the level of the distribution peak. Several other properties of this GFP “profile” can be used to find different information about the cells. This is described in more detail in Chapter 6. This new method is one of image pre-processing; to prepare images for segmentation by software, in this case, CellProfiler. It is not a method of segmentation, although as outlined in Chapter 7, it has the potential to become one.

## 1.3 Thesis outline

Firstly, a brief description of the microfluidics environment, its purpose, and its limitations will be given in Chapter 2. The system used and its properties are the original reason this study into image processing was undertaken. The 3D nature of the system prevents conventional 2D microscopy, and the live cell environment meant that more detailed cell fixing techniques could not be used. The lack of image quality and coarseness of the data led to the need to investigate if any useful information could be extracted reliably from it.

The current method depends heavily on the distribution of GFP within a cell. This, along with an understanding of cell shape and its optical properties and responses to the light used in the microscope is important for determining how useful this method can be in changing conditions. If the type of microscope or environment is changed, this method should be able to operate under a new set of parameters. A description of the places GFP can be found within a cell can inform adaptations of this method and help find conditions where the method could fail or have reduced effectiveness. An example of this is cytosolic versus cytoskeletal GFP, found in the central cytosol and the external cytoskeleton respectively. These two different distributions of GFP can effect this method which relies on peak positions of the profiles. Peaks in different distributions can give misleading answers regarding the positions of parts of the cell. A description of the brightfield reveals similar situations. A key example is the superposition of two objects in the environment. The brightfield light is mixed in the final data, so data representing superimposed objects cannot be divided into specific shapes of both objects. This limitation cannot be resolved with the GFP data. This and other problems will be described in Chapter 3.

To explain the context of this type image pre-processing, a background in image processing and some techniques used by CellProfiler will be given in Chapter 3. Basic image features can be combined into larger features that can delimit objects and parts of objects. Software like CellProfiler can use this information to measure shapes and other properties of cells in an image. It can also be used to track cells from one frame to another by looking for similar cell shapes and proximity. The method described here depends on the way a recognizer like CellProfiler works, although with further work, the information used for pre-processing in this method could allow a more powerful segmentation algorithm to be created. This will be investigated finally in Chapter 5.

Finally, testing will be used to compare this method to previous experimental work and commonly used methods of image pre-processing. Although this is not yet a fully capable segmentation method, the pre-processing can be compared by segmentation. Data from several experiments was collected and cancer cells within them segmented. Several properties

of the cancer cell shapes, such as the projected 2D area, can be used to compare images on their ability to represent the cells.

# **Chapter 2**

## **Imaging focus: the microfluidics environment**

### **2.1 Purpose and the need for segmentation**

The reason this environment was developed is to determine how cancer cells cross the endothelium (blood vessel wall cell barrier) during extravasation, or the stage of metastasis where cancerous cells that have already entered the blood stream from some initial location, make their way around the body, break through the blood vessel wall, and embed themselves in another type of tissue. Extravasation is a partially understood process in cancer biology [10], and this type of system could help to understand it by providing accurate data on the morphodynamics of the cells as they move in the simulation of a blood vessel.

To provide useful data, information about a great many cells must be gathered. This requires visually identifying cells and parts of cells and assessing their changing shapes, sizes, and speeds over time and in distinct regions of the environment. This can be done manually by keeping track of each cell and recording its progress over the course of the experiment. Unfortunately, this is impractical for the amount of data needed and would be too time consuming for a human to do. As such, it must be done automatically. This type of recognition done by a computer is known as segmentation, where cell shapes are separated and differentiated from the background. Many algorithms, techniques, and pieces of software exist to solve this with varying levels of success. They require a mathematical description of a set of images, and a way to consistently find features of the objects of interest that can be matched and measured.

Certain aspects of the environment used in the experiment and the methods by which it was imaged pose problems for accurate cell segmentation by disrupting the consistency

that cell segmentation algorithms depend on. Traditional cell microscopy using glass slides and chemically fixed cells allows for high resolution images of cells that are consistently in focus. Factors affecting the quality in this case are the 3D structure of the channel, the live cell environment where cells are free to move and interact, and the movement of the microscope hardware and cancer cells vertically (relative to the microscope objective) that causes object to fluctuate in and out of focus in the final data.

## 2.2 Confocal microscope and 3D structure

Image data were gathered using a confocal microscope. This allows a 3D space to be imaged by scanning over a volume and recording data at a number of discreet levels. Data can also be recorded in a number of different channels (the brightfield channel is shown below in Figure 2.1). The data for these experiments used brightfield, or transmission, images and GFP fluorescence images. The light in brightfield images from different levels is mixed (blurred) by the optics of the microscope objective, resulting in distorted representations of objects unless their level is in focus. In contrast, light from GFP inside cells can be isolated to a particular level using the pinhole mechanism of the microscope. The size of the pinhole determines the maximum resolution of the image. This isolation of the GFP channel levels can be used to build up a 3D model of the objects marked with GFP, which in this experiment is only the cancer cells. Cancer cells can then be distinguished from other types of objects in the experiment.

The 3D information from the GFP can be used to locate cancer cells within the environment, but the limits on the resolution prevent accurate outlines of the cells from being found. This is also dependent on the cells' internal distribution of GFP. The cancer cells in the current experiments had GFP embedded within the cytosol, or the fluid interior of the cell. From this, the general bulk of the cell and to a certain extent its general shape could be made out, but finer edges and protrusions could not be determined since the GFP did not penetrate the cytoskeleton or the outer wall of the cell. The method used to find cells and prepare the images for segmentation is directly dependent on the this arrangement of the GFP. modifications can be made to account for other sources of fluorescence inside the cell. This is discussed more in Chapter 3.

## 2.3 Description of the environment

The microfluidics environment used for this study consisted of a microchannel framework printed using soft lithography on a PDMS chip. PDMS, or Polydimethylsiloxane, is a silicone

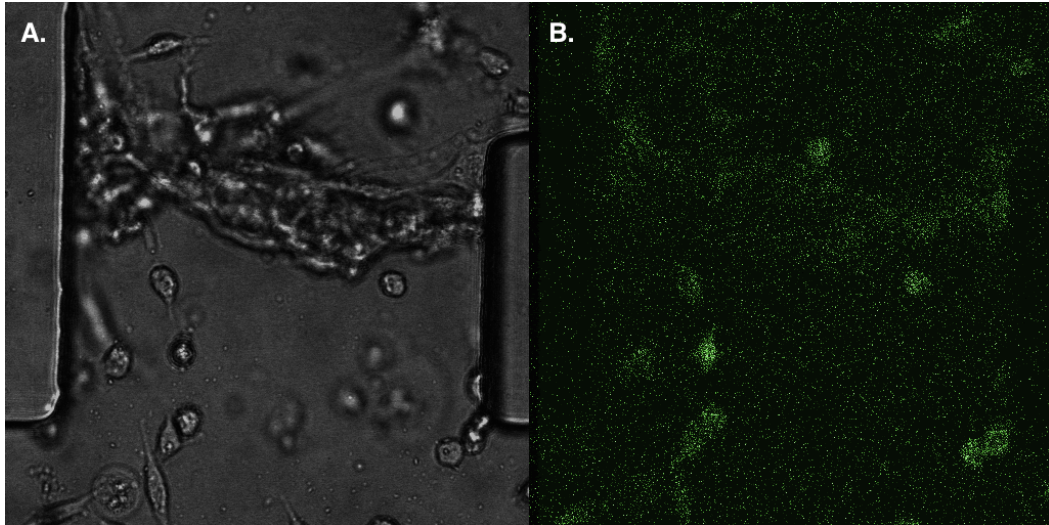


Fig. 2.1 This is sample of image data obtained from the microscope. Each image shows a single slice from a single frame in one series of an experiment. A shows the brightfield image, while B shows the GFP for the corresponding slice. The same physical space is represented by both images. This correspondence can be exploited to make use of useful information from both images.

gel that can be molded and used to create microscopic structures, such as microscopic channels to use as environments for cells [19][6][5]. This microchannel technique is seen as a potentially groundbreaking paradigm in the biomedical industry to mimic body tissue for complex *in vitro* studies. In this case, the channel was set up to model a human blood vessel. The diagram in Figure 2.2 below shows part of the channel framework with two PDMS pillars on either side of a gap. On one side of the gap, a liquid medium meant to simulate blood plasma is pumped in where it can remain static, or be used to simulate the flow inside a blood vessel. On the other side of the gap, collagen gel, used to simulate the extracellular matrix surrounding a blood vessel, provides an anchor point for the endothelial cells, or cells found in the blood vessel wall, to attach to. These endothelial cells are added to the environment prior to the experiment. The experiment is monitored when cancer cells that are marked with a fluorescent GFP, or Green Fluorescent Protein, are added to the environment in the medium channel, from which they can cross the endothelial cell barrier into the collagen gel, as they might *in vivo* during the extravasation stage of metastasis [10].

The entire channel is approximately 100 microns thick. this is roughly an order of magnitude greater than the width of a typical cancer cell used in the experiments. During the experiment the cells may be attached (flattened) and thus much thinner vertically. The width of the gap horizontally containing the endothelial cell barrier is between 100-200 microns. A typical blood vessel would be tubular, but this setup, while possible, would be difficult to study and to image with a microscope. Opting instead for the simplified setup, the vertical

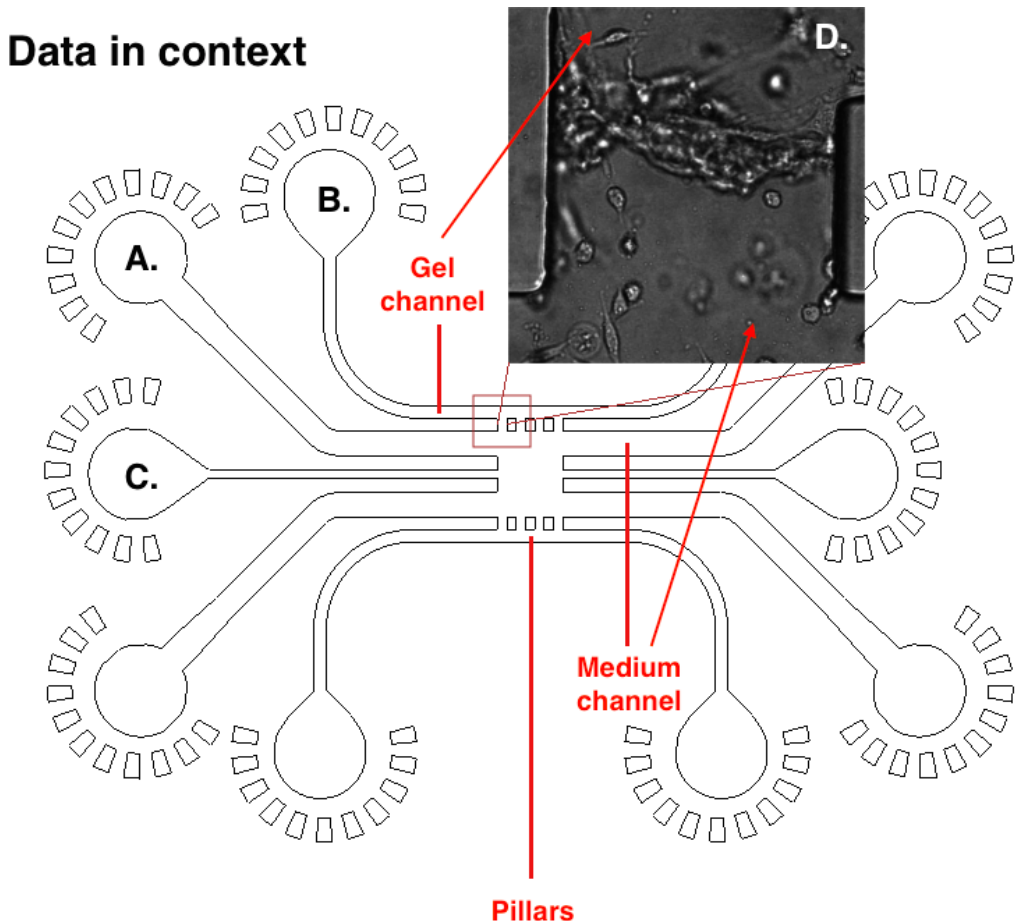


Fig. 2.2 This diagram shows a schematic of the microfluidics environment used in the current set of experiments and a small sample of data captured from it. The nodes at the ends of the channels (A,B,C) are feeds for the channels in the centre of the device. Liquid and cell matter can be placed in these feeds to seed the environment. Feed A leads to the medium channel adjacent to the pillars. Feed B leads to the gel channels on the top and bottom of the device. Feed C in the centre of the environment is designed to introduce drugs and other chemicals into the medium channel at the point of contact between the gel and medium (the pillars). The image D is the same data as shown in Figure 2.1, but placed in context of the device.

wall of cells can be observed much more easily and still be used to provide information on how the cancer cells cross the barrier. More advanced setups are under development at the time of writing.

## 2.4 Live cell imaging limitations

Imaging live cells imposes limits on the techniques available since the cells must remain alive and be able to behave naturally for the entire duration of the experiment. This means

they cannot be subjected to excess illumination from the laser used to stimulate fluorescence lest they absorb too much energy and overheat, causing erratic movements and finally death, making any data on their movements unusable. This limit on the amount of light that one is able to put into the cells to stimulate the GFP limits the amount of light that can be gathered from the cells. This lowers the brightness and contrast of the final data, making the location of finer details in a cell less certain.

The cells are also free to move about the environment. Tracking a single cell means it must remain in the field of view. The time period in this experiment necessary to allow the cells to cross the endothelial barrier is between 10-15 hours, and the distance a cell can move in this time sets a lower limit on the size of the viewport, or the view of the microscope that is finally recorded as an image. A large viewport means a lower resolution, since the objective must move away from the sample. This sacrifices image quality per cell for information about many cells. For this trade-off to be worthwhile, useful data must be extracted from the lower quality cell images. This is difficult for simple cell segmentation algorithms.

The movement of the cells is not restricted to the two dimensions of the viewport. The cells can move up and down in the environment (towards and away from the objective). This will move them between different focal planes. While all this data is recorded, cells cannot be guaranteed to stay on one level for the whole experiment. As a cell moves vertically, its representation in the image will change and properties of its edges will change their colour and texture. This breaks the feature consistency that segmentation relies on.

## 2.5 Autofocus and focal fluctuations

Apart from the behaviour of the cells, the microscope hardware must also operate reliably for the 10-15 hour time period. This is not always possible, and small changes in the alignment of different components will cause systematic errors to build up and compound over time. The result of the microscope imaging in one alignment while the instruments report another causes errors in the consistency of the image sequence. The focus will fluctuate visibly while an index representing the focal plane remains the same. This means such an index cannot be relied on to accurately report the location in the environment.

Software that is meant to solve this problem is known as Autofocus [3]. Most commercial microscope setups come with this software preinstalled. It attempts to analyse the images gathered at regular intervals, for example, every frame, and determine the current focal plane in the environment from simple numerical properties. An example of such a property is the minimum entropy of the image [3]. By keeping the minimum entropy constant, the image plane with the most similar entropy in the next frame can be found. This is set

as the corresponding level so that representations of the objects remain constant. Other methods such as measuring the reflection of light from the cover slip of the sample are also used [9]. Highly variable environments such as live cells can cause misleading calculations of a constant entropy, hence the unreliability of the level index. This makes segmentation more complicated.

# **Chapter 3**

## **Background**

### **3.1 Introduction**

A comprehensive background on the key concepts that the method presented in this thesis is based on is essential for understanding its context and significance. Any physical or mathematical principles that might affect the performance of the method should also be understood. The previous chapter outlined some of the problems faced when attempting to segment cancer cells given a 3D live cell environment. These included autofocus fluctuations of the microscope and limits on light absorption by cells. This chapter gives some detail on topics including the GFP distribution within the cells, which plays a key role in the pre-processing method, basic image processing and segmentation and how these techniques are used in CellProfiler and other segmentation software packages, and finally an introduction to the brightfield method on which the current method is based.

### **3.2 Cell microscopy, optical structure, and GFP distributions**

Under a microscope, the visible parts of a cell, the optical properties of edges, and colours observed depend on the materials that it contains. The material in a typical human cell has a refractive index similar to that of water, making it colourless and transparent [8]. But, when light passes tangentially through the cell membrane, it can be blocked and give the appearance of a dark edge. This leads to a projected (2D) shape under the microscope. This shape is a closed curve and thus has an interior (the material within the cell) and an exterior (the background). This is an assumption made throughout the segmentation process, since it is not possible for the cell to be an open shape. This is useful for segmentation, because

there is a natural boundary that allows the recognition to be restricted to closed curves made up of dark edges.

Cells can move in response to chemical stimuli [13]. In order to move in their environment, a cell can change tension in its outer membrane and form protrusions that stretch in the direction of a stimulus [13]. This can allow the cell to propel itself and follow chemical gradients. These protrusions, if they can be measured, provide useful information about the behaviour of the cell in response to any agents that have been added to the system as part of the experiment. The microfluidics environment was designed with the addition of chemical agents in mind. Even without added stimuli, the purpose of the experiment is to be able to observe the cells moving and allow for their shapes to be measured. Accurate recognition of cell protrusions is a key aim of this study.

Cells can be marked by injecting a variety of fluorescent proteins into different parts of their internal structure such as the internal cytosol, the cell membrane, and the nucleus. A common protein used is known as GFP, or Green Fluorescent Protein. It can be expressed in the cytosol, a clear fluid surrounding the nucleus, occupying the bulk of the cell, but made to exclude the membrane or the nucleus [20]. When a 3D reconstruction is created using a confocal microscope, this distribution of GFP will appear as a single bulk shape with a gap at the location of the nucleus. It notably does not contain information about the extremities of the cell such as protrusions. It can also be expressed in the cell membrane, leading to a hollow 3D shape that shows clearly the extremities of the cell. This variation can affect the method of image processing used, as shown in Figure 3.1.

### 3.3 Image processing and segmentation

One of the most important features that can be extracted from an image is the location of edges. They delimit objects and provide evidence of texture within an object. An edge is defined as an intensity discontinuity in one dimension [18] [11]; a straight line between areas of different colour. Crossing the edge, the intensity or colour can be plotted and represented as a mathematical relationship between the intensity and the path taken. Movement across a thin dark edge between two regions of similar intensity will show a decrease in intensity followed by a subsequent increase once the edge is passed. This is dependent on the image, but a robust mathematical model allows edges in a set of images to be found quickly and reliably. The ability to rapidly find edges in an image is a key tool in a segmentation program, since this is the most certain way of locating objects. An example of a widely used edge detection method is called the Canny filter. Proposed by John Canny in his 1986 paper, *A Computational Approach To Edge Detection* [1]. It works by first smoothing the image to

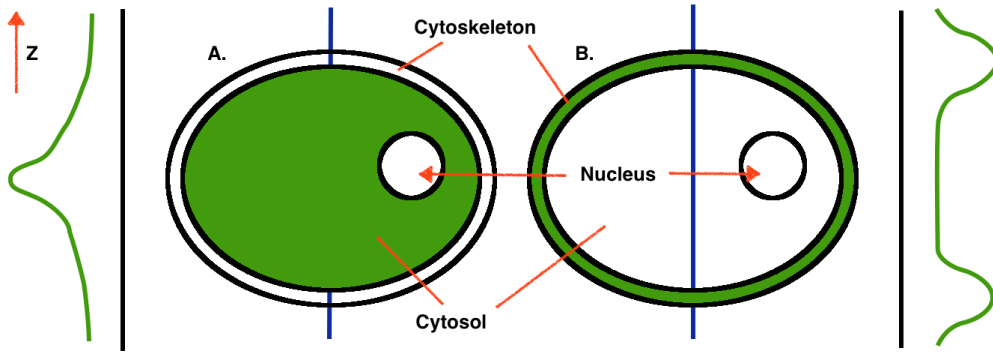


Fig. 3.1 Different parts of a cell are composed of different materials that can be made to bind with fluorescent proteins such as GFP to highlight the cell structure in a microscope image. For example the skeleton of the cell and the outer membrane are composed primarily of actin filaments. The membrane is marked as the cytoskeleton, but in reality it extends throughout the cell in filaments. This method relies on a consistent formation of the GFP inside a cell. This current method expects a single peak for the centre of the cell, such as in A, since this type of staining is used in the experiments. Note the lack of GFP expressed in the nucleus. It could be made to bind with the cytoskeleton, such as in B. This would produce a vertical intensity profile along the blue line similar to the plot on the right with two peaks. The method would have to be modified to account for these types of changes.

reduce noise, finding the intensity gradients of the image (edges will show a high intensity gradient), suppressing points with less than the maximum gradient, along with applying an absolute intensity threshold, and finally joining potential edge segments by removing those not connected to strong edge segments. Other features such as corners can be modelled as superpositions of the simple edges in different orientations. An example of the results of this process can be seen in Figure 3.2

Here is a list of steps to complete the Canny algorithm:

1. The image is smoothed using a Gaussian kernel of the form, with size  $2k + 1$ :

$$H_{ij} = \frac{1}{2\pi\sigma^2} \exp\left(-\frac{(i-k-1)^2 + (j-k-1)^2}{2\sigma^2}\right) \quad (3.1)$$

2. Find the intensity gradient of the image in 2D (both magnitude,  $G$  and direction,  $\Theta$ ).

$$G = \sqrt{G_x^2 + G_y^2} \quad (3.2)$$

$$\Theta = \tan^{-1}\left(\frac{G_y}{G_x}\right) \quad (3.3)$$

3. Perform non-maximal suppression on the resulting gradient image. This is done in two stages:

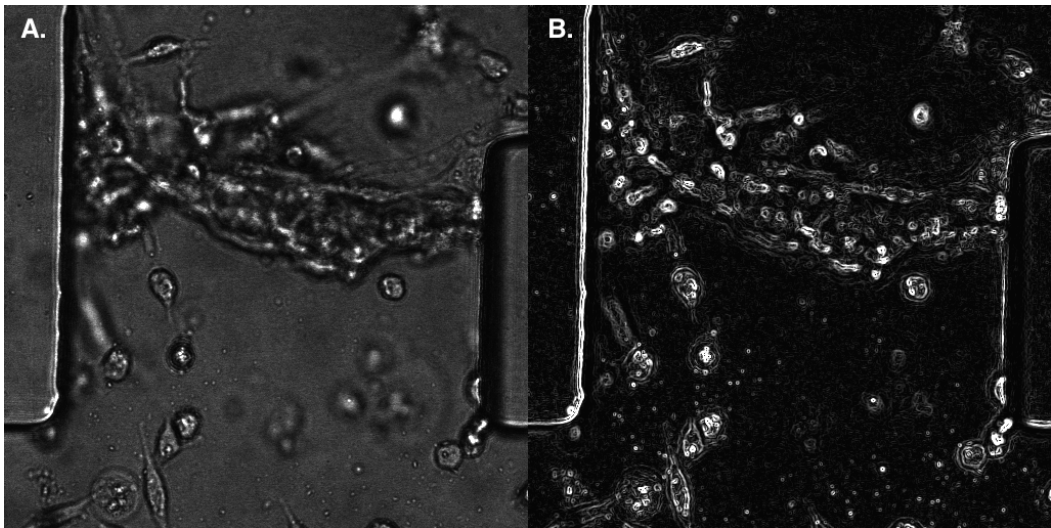


Fig. 3.2 By analysing the intensity gradients in an image, the Canny edge filter highlights the points with the highest intensity discontinuities. These appear as the edges of the image in the above example. The image in A shows the original image. B shows the edge filter applied to this image. Clearly, areas of continuous colour, such as the background do not contain edges. This image alone gives a good indication of where to look for objects.

- (a) Compare the edge response of each pixel to its nearest neighbours in each gradient direction.
- (b) If the value of the pixel is greater than its neighbours, preserve it, else suppress it.
- 4. To suppress any pixels left over after non-maximal suppression due to noise or other random colour variations, apply a double threshold to the resulting image. This is normally done using the Otsu method [14], which minimises the variance between two classes of pixels, a Foreground, or cell objects, and the Background.
- 5. Lastly, complete any broken edges using Hysteresis. This processing searches for objects in the image and attempts to incorporate weak edge pixels into the final edge image. This is done by looking at all eight neighbour pixels (a single pixel has eight immediate adjacent neighbours) for a weak edge. If at least one strong edge pixel is found, the weak edge pixel will be preserved.

Another tool for recognition is the blob detector. A “blob” is a technical term meaning an contiguous (interconnected) region of uniform (similar) colour. This could indicate a solid object or a region of background. Depending on the type of imaging, blobs that represent objects can either be light or dark, but both can be found by modelling the region as a 2D intensity discontinuity. This can be represented mathematically as a 2D Gaussian of arbitrary, but fixed, radius. Such a modelling function can then be convolved with the image in a

similar manner to simple edges. Parts of the image that contain regions of colour of size proportional to the radius of the Gaussian will give a response to the convolution. The areas with the highest response are the most likely candidates for objects of the specified size. A sample of this sort of algorithm is shown in Figure 3.3. Bright areas could be possible candidates for objects.

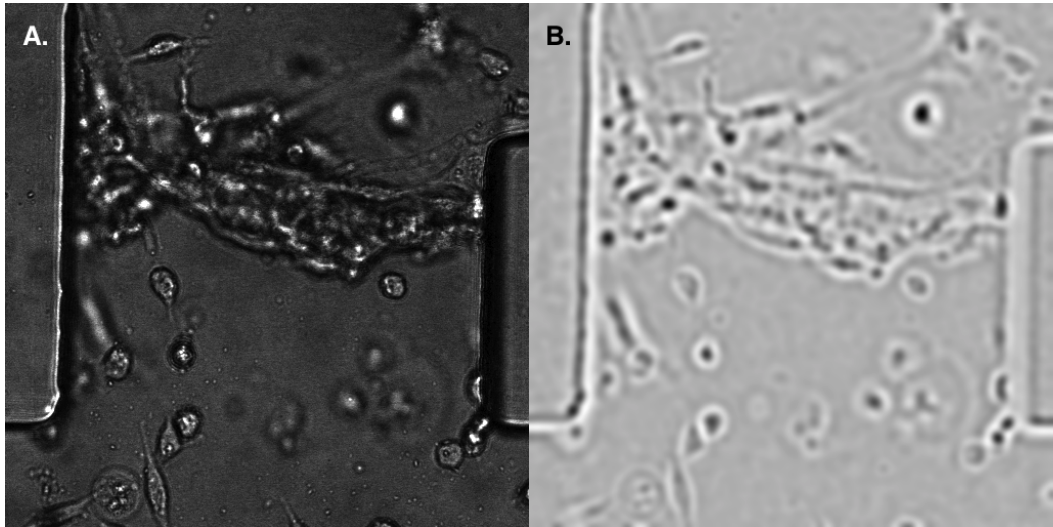


Fig. 3.3 Blobs, a technical term, are regions of contiguous (or interconnected) similar colours. Boundaries between these regions are edges and can be found using an appropriate filter as before. Blobs are found by convolving the image with a choice of filters. This image, A, was convolved with a simple Difference of Gaussians (DoG) curve, a shortcut for approximating a Laplacian operator, which in turn approximates the intensity profile of a blob with edges in XY. Blobs that match this profile (most importantly its size), will give a similar “response” and appear brighter in the final image, B.

Once blobs and edges have been found, it is possible that in a given cellular environment, cells will be found packed closely in dense clusters. In order to be differentiated from each other, boundaries between the cells must be drawn based on the image properties surrounding them. Often, cells are separated by sharp discontinuities such as dark edges, but they may be so close that optically, their intensity curves appear to transition smoothly from one cell to another. In this case, a variant of the watershed method is useful for separating them [7]. like many image processing techniques, the watershed method models the intensity map of the image as a terrain, where the contour height at a point is proportional to its intensity. If one imagines the terrain as being slowly filled with a certain amount of water, highly divergent regions such as cell representations will stand out like hills and the point where each “hill” meets the water is the boundary of that cell. If the water is raised high enough, even smoothly transitioning boundaries between cells will appear to have a dividing line between them. This can be used to segment closely packed objects using their intensity peaks alone. An

example of an attempt at this algorithm is shown in Figure 3.4. There might not be enough information in the image other than a size estimate of objects to draw true dividing lines. Several objects may appear divided into a number of chunks. Parts of the background have also be divided, again due to lack of information.

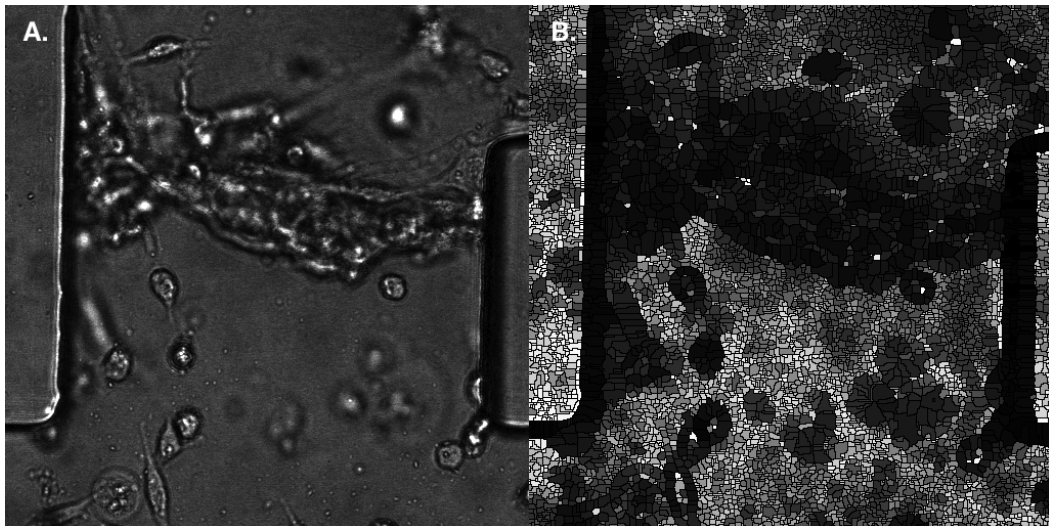


Fig. 3.4 The watershed algorithm can be used to separate neighbouring objects by analysing the intensity curve joining their centres. If there is an inflection point in the intensity curve between them, it can be used to draw a line separating them. B shows an example of this type of algorithm applied to A, the original brightfield image. Parameters can be varied controlling the size of the objects separated to better estimate the types of curves that should be prioritised.

A watershed algorithm was proposed by F. Meyer in 1990. The steps for the watershed algorithm are as follows:

1. Choosing starting points for the watershed. “Water” will “flow” from these points. These can be positioned at the maxima in an image, randomly, or in a grid. Each is given a different label (a simple integer value).
2. Each iteration, the neighbours of the marked pixels are placed into a queue and ordered by a priority proportional to their grayscale values. There will be one queue per label.
3. The neighbours of lowest priority pixel from each queue are checked. If they are all marked, the lowest priority pixel is marked with their label. Any un-queued neighbouring pixels are then queued.
4. Repeat step 3 until all queues are empty.

## 3.4 CellProfiler and segmentation software

The last section details some of the methods used by CellProfiler and other software packages, such as several ImageJ plugins, to segment cells. When CellProfiler is provided with an image, depending on the module used for analysis, it can first look for blobs of colour in the image. Dependent on the background, it will look for bright or dark blobs as potential candidates for objects. The edges close to these blobs are kept as potential object edges. The blobs of colour are then separated using a watershed method. Their contours are matched with the edge image and the space is filled in to form an object "mask". The mask is a binary representation of the object of interest, an example of which is shown in Figure 3.5. Every point in the mask is considered part of the object, and all points outside are considered part of the background. The watershed method allows adjacent masks to be separated. Every task that CellProfiler performs on an image such as edge detection or blob detection is typically contained within a module that stores information about operations done to the image. These modules can be chained to compound effects and allow very specific workflows to suit all types of images. It can also combine images from several channels using basic mathematical operations.

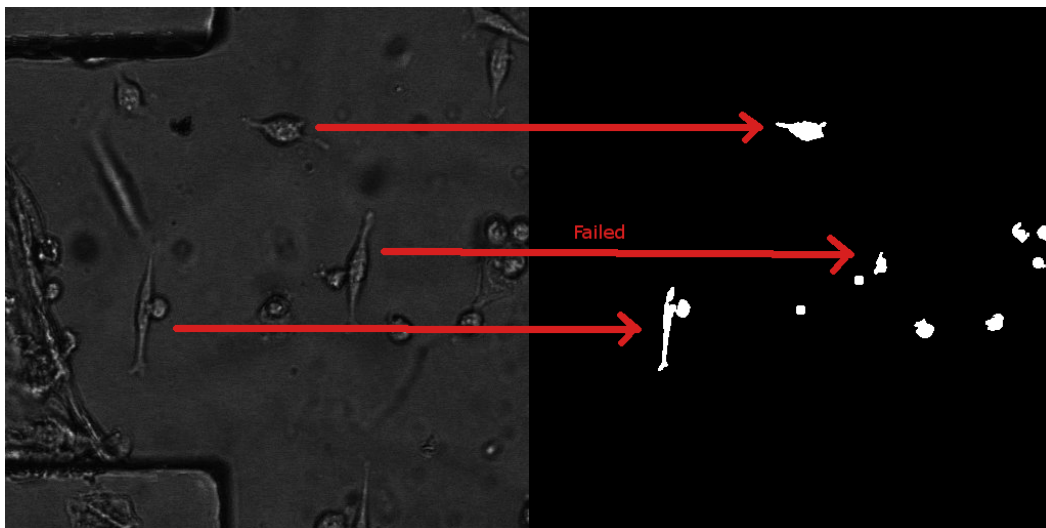


Fig. 3.5 A mask is the general term for a binary representation of an object. Pixels inside the mask, marked variously as white, true, 1, or 255, represent parts of the image that lie inside the object of interest. Pixels that are black, 0 or false, lie outside the object and are considered part of the background. If multiple objects are contained within the same mask image, they can be marked with a different integer label such as 2, 23, 44, etc. to allow them to be differentiated. They may have previously been separated using a watershed algorithm or similar. By marking them with a unique grayscale id, they can be individually extracted from the image and observed. The examples given in B are typical outputs from cell recognisers such as CellProfiler.

CellProfiler has a particularly useful module called “Secondary Objects”. Rather than searching the image for objects from scratch, it can use information about previously found objects to search in their vicinity. If object centres are represented as points, Secondary Objects can search around the points and use information about the vicinity of the point to match similar patches of colour or edge profiles. This operation is very adaptable, and does not have a size preference, filling whatever space is available. This is highly valued since one of the driving philosophies of this work is that recognition should not be biased towards a particular size or shape. A disadvantage of this approach is a recognition that expands without limit. If there is no discernible boundary, there is no reason for the recognition to stop expanding into the background if it is of similar intensity. This can be seen in Figure 3.6. To clarify, if the background of the image and the interior of the cell have similar colours, and the edges of the cell are incomplete or have an inconsistent profile, the recognition could add parts of the background to the final mask of the cell. This can affect the method used, but eventually adding 3D information to this 2D method can solve the problem.

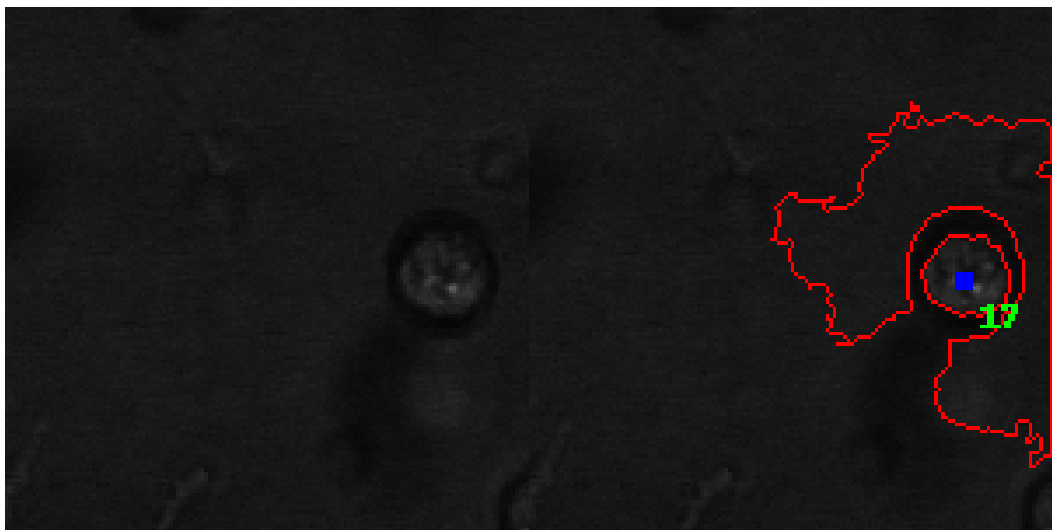


Fig. 3.6 The Secondary Objects module in CellProfiler can cause errors in the recognition. In this case, the colour of the interior of the cell is very similar to that of the background. They are separated only by the dark colour of the edges. If there is a gap in the edge, or some interaction with exceptions at the edge of the image, the boundary separating the interior of the cell from the background can be poorly visible, allowing the segmentation to “spill” from the previously marked interior into the background. This leads to results such as B. This causes the area or other numerical properties of the cell recognition to be overestimated and calls into question the utility of the recogniser.

Another tool for segmentation is the Blow/Lasso tool in ImageJ. This is based on the LASSO (or Least Absolute Shrinkage and Selection Operator) algorithm [15] [17]. LASSO is a least square regression algorithm that treats the image as a “terrain”, where the “height” of a pixel is proportional to its intensity. If an algorithm follows a path through the image,

moving from one pixel to another can be assigned a cost based on the relationship between the intensities. An algorithm could be set up such that moving into dark edges could be very cheap, but moving out of them could be expensive, causing the path to follow a chain of edges closely. In a similar fashion, two points can be specified and the cost between them calculated [15], shown in Figure 3.7. If one point is specified as the centre from which to search, the locus of points that share the same cost from the centre can yield a closed shape with dark edges such as a cell. While not reliable without tuning, the cost function can be made more specific to suit the application. Such a function can also be made to take account of multiple channels. Depending on how it is implemented, considering a central point can bias the shape towards a circular locus.

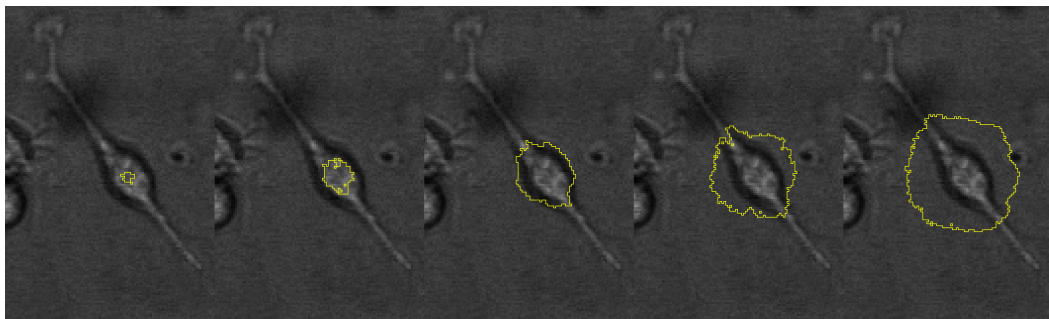


Fig. 3.7 The LASSO algorithm, implemented in ImageJ as the Blow/Lasso tool, traverses the images from a centre to a test point and matches other points and paths in the image around that point that share the same “energy”. This can be used to closely fit the edges of an object, as the algorithm will avoid entering edges and other dark features. This can be used as a form of segmentation given a starting point.

A notable disadvantage of CellProfiler is the lack of comprehensive support for 3D environments and sets of images with 3D relationships. Although it can be made to behave in this way, images must be processed on an individual basis or in basic groupings, limiting the complexity of 3D operations. This makes true 3D segmentation difficult or impossible. Nevertheless, CellProfiler has a wide array of very powerful 2D operations. Thus an ideal solution is a method that is able to cast a 3D dataset in a 2D context in order to take advantage of 2D methods while preserving 3D data.

The final data output from CellProfiler is a list of object masks along with some analysis [???] of their shape such as their eccentricity or orientation (from a bounding ellipse). CellProfiler does allow the segmentation of connected objects, such as protrusions, and can provide their measurements, but this can be unreliable since the properties of protrusions are hard to specify. A larger problem with CellProfiler is the inability to adapt to inconsistencies. For example, the edges of a cell protrusion can have a very different appearance to the main body of the cell as the cell membrane grows thinner. A cell protrusion is defined in this

study as an extension or stretching of the cell membrane used by the cell for movement. An example of this movement is shown in Figure 3.8. Although no research was done for the purposes of this study on the correlation between protrusion formation and cell movement, this type of study can be done easily using the resulting software. However, while the edge of a protrusion maybe remain visible towards its apex, the difference in edge properties might cause CellProfiler to conclude that they are unrelated edges, and lead to a protrusion being rejected and not represented in the final data. This unreliability with regards to “tertiary object” like protrusions is insufficient for the accuracy required by this project. The method in Chapter 5 will show how 3D information can enhance the recognition of tertiary objects.

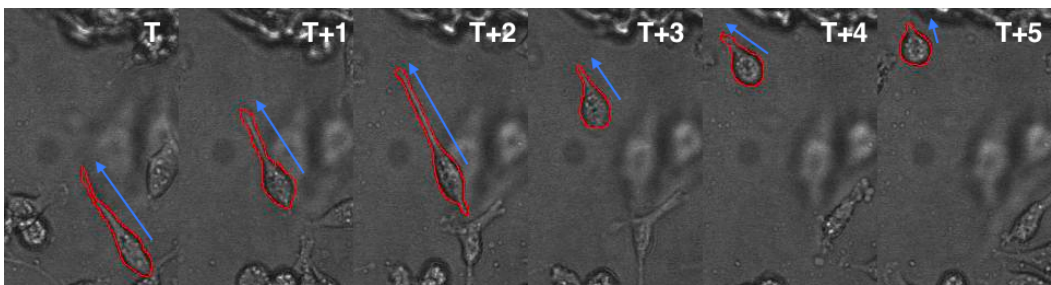


Fig. 3.8 The cell membrane is a malleable series of interconnected proteins that can respond to a variety of chemical gradients. A typical response can take the form of a “protrusion”, which extends from the cell in a particular direction, usually in the direction of a stimulus. The cell depicted here is using the protrusion to move from the bottom of the image to the top. The approximate length and orientation of the protrusion is marked with a blue arrow. The protrusion first extends and then retreats as the movement is completed. Any useful cell recognition tool must allow such cell features to be tracked and measured. This is a key goal of this study.

### 3.5 Cell tracking

Cell tracking is any method of associating recognised objects in different images gathered at different times and assigning them same identity. This can allow properties of the cells such as area and position to be plotted over time and for trends to be observed. In a low density packing of cells, this can be as simple as finding the distance between objects in different frames and assigning the next iteration to be the object with the smallest distance from the starting point. In this study, connected iterations of a single physical object are referred to as “instances” as in “cell instance”. This is an important distinction, since a cell objects cannot be said to have an area or velocity since these properties change with time. Velocity also requires multiple frames to determine, so intermediate velocities can be assigned to the cell instance rather than the cell. Assigning an area to a particular cell at a point in time is

equivalent to assigning the area to the cell instance. Thus a single cell can have many cell instances.

A popular tracking method is the LAP, or “Linear Assignment Problem”, framework tracking algorithm. Once two lists of objects and their positions in subsequent images are found, they can be connected and ranked by a likelihood of correspondence. This is done by first constructing and solving a NxN [maths] matrix of correspondence parameters where N is the number of objects considered. A similar matrix is constructed to represent the probabilities of cells merging or splitting. The final step reconciles the two images into a list of corresponding cell instances. This process can then be repeated for subsequent frames. This algorithm is employed by CellProfiler as a module, so it can be applied to objects found through recognition. Other properties of the cells such as changing shape and size can contribute to the likelihood of correspondence. LAP also helps to associate cells that disappear and reappear, as well as cells that merge or split.

The method yields four important numbers, namely “LostObjectCount”, “NewObjectCount”, “SplitObjectCount”, and “MergedObjectCount”. A measure of the reliability of the tracking is given by the consistency of these numbers. For example, if NewObjectCount continues to increase throughout the time series, it is likely that objects that should be connected are being rejected and treated as new objects. This can happen if objects move a long distance, such as many multiples of their length, between frames. If the ratio of distance moved to time between frames is too high, the tracking algorithm may be too unreliable for use. Due to this unreliability, manual tracking is necessary to provide accurate information about cells. Manual tracking is used throughout this study, but further possibilities for automatic tracking can be derived from the current research.

## 3.6 The Selinummi brightfield profile method

In their 2009 paper, Bright Field Microscopy as an Alternative to Whole Cell Fluorescence in Automated Analysis of Macrophage Images [italic], Selinummi et al. describe a method of using 3D brightfield information to aid segmentation instead of relying on GFP imaging of cells. The images for their study were gathered in a similar way to this study. A confocal microscope was used to scan a 3D environment gathering images in brightfield and GFP channels. Gathering data with a confocal microscope is slow and expensive, so if adequate cell data can be produced using a single channel, this can save time. They proposed using the amplitude of the variation of the brightfield intensity in the Z dimension as an indicator of the presence of an object at a particular XY location. This exploits the behaviour of the brightfield representations of objects as they move in and out of focus. As outlined in Chapter

3, the brightfield does not store 3D information, but changes with the focal plane of the environment. An area of background will not vary across focal planes, but a location or single pixel containing an object will vary with focal plane.

The basis of the method is an inspiration for the current project. The vertical distribution of the brightfield intensities at a particular XY location, known as a “profile” in this study, shows how the features vary in intensity across Z. An example of these types of distributions can be seen in Figure 3.9.

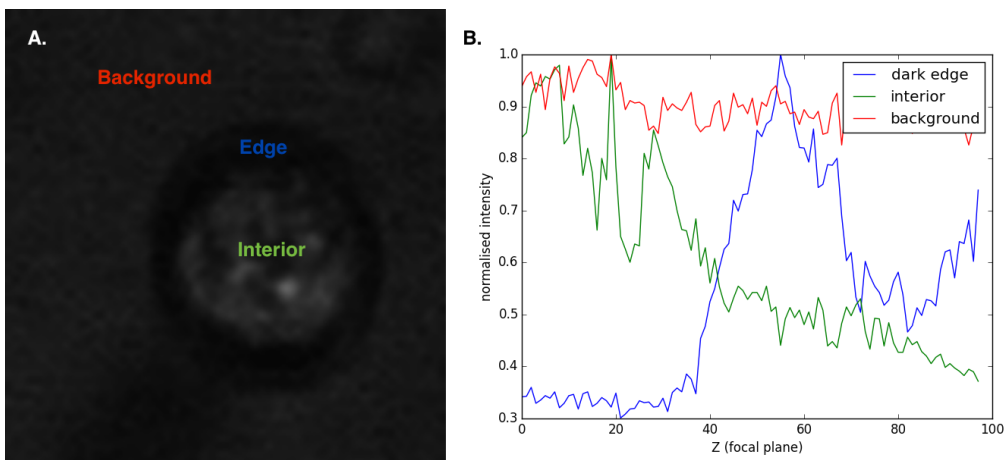


Fig. 3.9 The brightfield profile was shown by Selinummi et al. to be a powerful indicator of the presence of an object in an image. The profile for each pixel in XY is the intensity distribution of the column of pixels in Z. For three typical points in an image of a cell, A, the background, the edge of a cell, and the interior of a cell have very different profiles, seen in B. These differences can be used to separate parts of the image that can contain cells from those that contain only background.

Their results were promising for the data they gathered, but suffered when applied to the data from the current experiment. To test the method, they compared cell segmentation of the modified brightfield images to the GFP images of the same cells. They used the GFP segmentation as the “ground truth” of their testing. Ground truth is assumed to be the best representation of the object. This is a failing of the study since there are many details omitted by the GFP, especially considering the variety of configurations cellular GFP can take. Segmentation was compared pixel by pixel using the “FScore”, or a compound ratio of the true and false positive scores, given by:

$$\text{Precision} = \frac{tp}{tp + fp}$$

$$\text{Recall} = \frac{tp}{tp + fn}$$

$$F\text{Score} = \frac{2(Precision \times Recall)}{Precision + Recall}$$

where:

1.  $tp$  is the number of True Positive, or correctly recognised pixels in a mask, according to the ground truth, or accepted best measurement of the cell.
2.  $fp$  is False Positive, or falsely accepted pixels.
3.  $fn$  is False Negative, or pixels falsely rejected from the mask.

FScore serves as a means of judging the accuracy of a mask from a certain algorithm in one single value.

There are several disadvantages of the Selinummi method, especially when applied to the current data. Firstly, the method was originally applied to a single cell environment with no visible materials other than cells. In contrast, the current environment is primarily composed of PDMS plastic. It is also a multicellular environment. The images thus contain many other objects in the brightfield that are not desired as part of the dataset, but they still have similar edges and strong variations in their intensity profiles. Regions of the image where any kind of object is found will appear bright. This can hinder accurate segmentation since unwanted objects are highlighted. Secondly, due to the brightfield variation in the images, strongly varying pixels can occur outside the true edge of the cell, causing these regions to be highlighted, and giving the cell a bright halo. This halo is picked up in the recognition and contributes to the measured area of the cell. This can cause an over-estimation of the cell area and a false representation of the cell's shape. These problems must be addressed for a variant of this method to be useful.



# Chapter 4

## Methodology

### 4.1 Introduction to the method

This method is a successor to the Selinummi brightfield method described in the previous chapter. An aim in developing it was to improve on two key problems. The first was the unwanted highlighting caused by objects other than those stained with GFP, preventing accurate segmentation of a multicellular environment. The second was a halo effect on the cells as the variance of the brightfield extended beyond the true edge of the cell due to blurring of the light in the brightfield between levels. The Selinummi method was originally intended to replace GFP segmentation in 3D environments [12]. This was previously done by projecting the GFP in the Z dimension, creating a new image where the value of each pixel corresponded to the sum or mean value of the pixels in that single XY profile distribution.

The concept of this method is, instead of disposing of the GFP, to apply the variance method previously applied to the brightfield to the GFP itself. This yields a much more informative estimate of the position and shape of the cell. Due to the low quality of the GFP, the precise shape of the cell cannot be found, but the 3D information can then be used to search the brightfield data and construct an image such that every object of interest (marked with GFP) appears to be in focus. This is in effect a method of pre-processing, since the segmentation can then be done on the product by CellProfiler or by other means in the manner of any other 2D image. In other words, the method proposed in this study casts 3D data in a 2D format that can be easily processed by well tested 2D algorithms. The method depends on three main parameters that can be varied to suit the application:  $R$ ,  $\Delta Z$ , and  $\Sigma$ . The next few sections will describe these parameters and their functions. They affect the linear smoothing of the original data, the focal plane of the outcome, and the final inter-level smoothing respectively.

While this projection of 3D data into a 2D context is the main method proposed, a further method of optimising the segmentation of the product using additional 3D data is included as it is important to the testing of the method. This optimisation uses the creation of artificial edges drawn on an image delimiting the boundary for cell segmentation of single cell or group of cells to prevent the segmentation of areas of the background with similar intensity profiles but low GFP intensity. This is an improved alternative to simply highlighting areas of the image with the highest GFP intensity.

## 4.2 The GFP profile

The key component of this method is the GFP vertical intensity distribution or “GFP profile”. For a single pixel in XY, this appears as a single series of intensities spanning Z. These values can be smoothed both in XY and Z. Smoothing in Z is meaningful because of the spatial relationship between planes of GFP in the environment. Planes in the brightfield are not related spatially, as thus cannot be meaningfully smoothed. Any noise present between frames in the GFP can be minimised and properties such as the maximum value can be determined to sub-pixel accuracy via interpolation. A profile can also be found by considering a square or mask of pixels in XY combined through some operation such as a mean value for each Z level. The size of this mask can be set arbitrarily to the size of a part of a cell, but as can be seen in Figure 4.1, such a method of generating the profile amounts to a type of linear image smoothing and yields a profile with similar properties to a profile generated using only the centre point of the mask. A size of between 3 and 5 pixels was chosen for the mask,  $A$ , to allow smooth transitions in the final image. This parameter is important to the outcome of the method and is given the symbol  $R$ . The function form of the GFP profile can then be given as:

$$G(z) = \frac{1}{\max(x \in A(z))} \sum_{x \in A(z)} \frac{x}{R^2} \quad (4.1)$$

where:

1.  $z$  is the vertical slice index in the image data.
2.  $R$  is the chosen radius of the linear smoothing kernel around the chosen location.
3.  $A(z)$  is the square of pixels defined by the size of  $R$  found at level  $z$ .
4.  $x$  is a single pixel in the area  $A$ .

Similarly to the brightfield profile considered by Selinummi et al., measureable properties such as the variance, the location of the maximum value, and the mean value can be found for

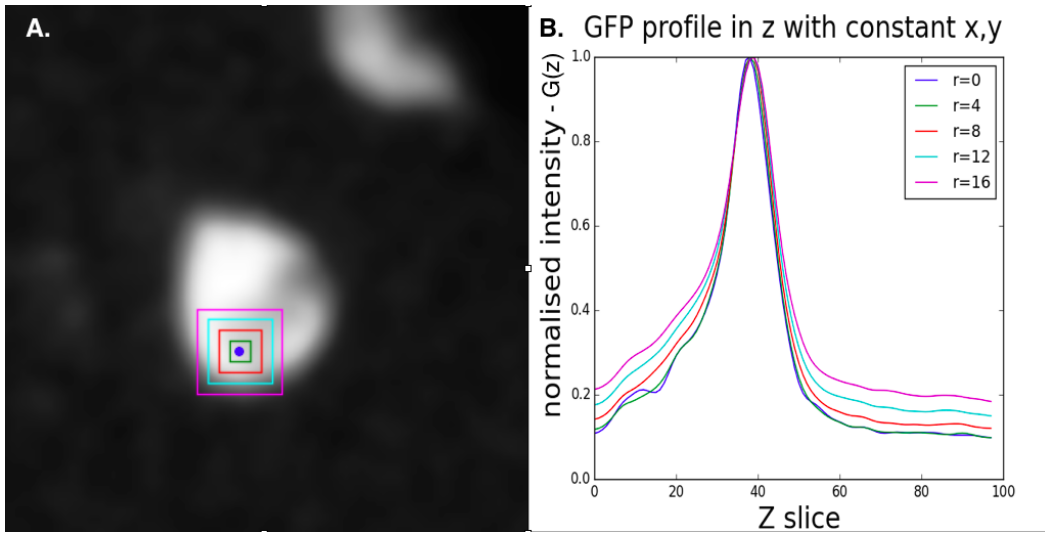


Fig. 4.1 Similar to the brightfield profile shown in Figure 3.9, a profile can be generated for the GFP. This might seem to trivially be the presence of GFP at various levels since the GFP contains 3D information, where the brightfield does not. Instead, these GFP profiles can be used to interact with the brightfield, which is limited in 3D. The goal is not to segment the cell in 3D using only the GFP. In the same way as Figure 3.9, three typical points show very different profiles. These can again be used in the same way to help tell the difference between different parts of the image. A shows the smoothed GFP of a single cell. The blue point is a single pixel. The coloured outlines show different radii around this point in XY. B shows the normalised distribution of GFP intensities in Z. The value at each Z is the mean or sum of the pixel values within the area of the outline, or A, as shown in equation 4.1.

the GFP profile. The variance was found using the normalised profile, that is, the maximum value in each individual distribution is set to 1. Comparing profiles in an image can then be done using their mean value and variance. These are linearly related as shown in Figure 4.2. A background pixel will have a flat profile, giving a low variance and a high mean, since the majority of the distribution stays close the maximum value. As peaks appear in the profile due to the presence of objects, the mean will decrease, but the variance will increase proportionally. In this way, pixels with varying profile strengths can show very clearly whether they contain an object. Figure 4.2 also shows a collection of blue points indicating points manually chosen to be inside cells. These are clustered in the high variance - low mean portion of the plot. The large cluster of points at low variance represent background pixels.

The most important part of the profile for the main method is the Z position of the maximum value. This indicates the peak intensity in the profile, and points to the most likely Z position of the part of the cell that contains the pixel in XY. This value can be used to search in the brightfield for an accurate cell representation by looking at the same level

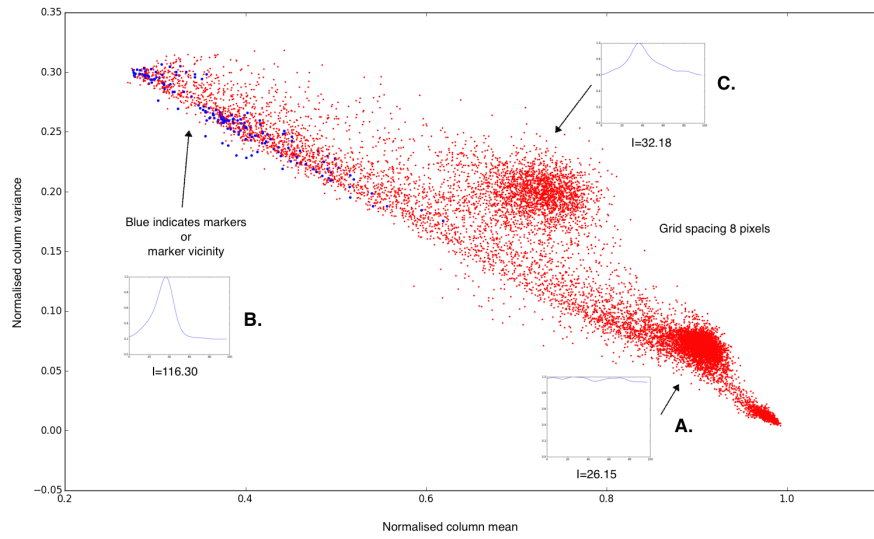


Fig. 4.2 Following on from Figure 4.1, different numerical properties of the profiles can be used to separate parts of the image. This plot shows a sample of points placed according to their mean and variance in intensity for different XY positions in the image. Profiles are normalised to their maximum, so a very high mean indicates a very flat distribution, e.g. A. A very high variance, as in B, shows the presence of an object. C shows edge pixels. Each red point represents a randomly sampled point in XY. Each blue point represents a manually chosen point observed to be inside a cell in the environment. The blue points are clearly clustered towards the top left, or the high variance side of the plot. This variance will be used to later to outline cells and the provide a maximum boundary for segmentation.

for the object in focus. Since the level indices are integers, the Z image was chosen by rounding the estimate of the Z position from the profile to the nearest integer. The more precise information is lost in the final image, but it can be stored elsewhere for further use.

### 4.3 Optimum features for cell recognition

By searching the brightfield image with the GFP profile, the goal is to find the optimum features for segmentation. These include bright, smooth, uniformly coloured interiors surrounded by consistent, dark edges. Given a series of focal planes showing the object, it is likely that there is a single plane that contains the closest possible features to the ideal features required. This is assumed to be where the maximum GFP occurs. Unfortunately, the location of the maximum GFP for a cell shows an image that is ironically “too focussed”. When in the sharpest possible focus, a cell’s edges become very thin and bright. To provide a better image for segmentation, a constant value is added to the level determined by the GFP

profile. This was determined empirically and set to be between 4-8 levels added to the profile estimate. This is the second parameter for the method and is given the symbol  $\Delta Z$ .

For manual tracking, the accurate shape of the cell does not need to be known; it is better to see the interior of the cell clearly in order to make a good estimate of the centre to place a marker. The focal plane best for this type of observation also does not lie on plane with the maximum GFP. This shift is also empirically determined and is between 10-12 levels above the maximum GFP. This parameter is not crucial to the outcome of the method and is set by personal preference of the user tasked with finding the cells.

## 4.4 zMod and zBF

For each frame in time, the Z position of the maximum of the GFP profile is calculated for each pixel in XY. A new image is created, called “zMod”, shown in Figure 4.3, where the value of each pixel proportionally represents a Z position in the environment. This is analogous to a terrain. The range of values lies between 0 and 1, but the intermediate values are discretised to multiples of  $\frac{1}{\text{number of ZPlanes}}$  in order to represent the full Z range of the experiment. Floating point representation is easier to keep track of than integer representation in an image since the float value also works as a percentage height in the environment. This map of Z positions can be smoothed to make transitions between levels more gradual. This is the third important parameter and is given the symbol  $\Sigma$ . In the present dataset,  $\Sigma$  is set to be a 3 pixel radius.

The zMod image for each frame can be mapped to the entire set of brightfield data for the same frame by selecting a pixel value from the brightfield stack focal plane that corresponds to the Z index indicated by the zMod image. This produces the most important result of this study, the “zBF” image, shown in Figure 4.4. It is a single 2D image for each frame containing representations of all objects in focus with clear edges and interiors. This works by only selecting pixel values from the levels where the objects are in focus. This does not correct the focus of objects not marked by the GFP. This image is used to segment all cells in the environment simultaneously independently of their level in the experiment using 2D segmentation techniques.

## 4.5 Artificial edges for segmentation: zVar and zEdge

A further improvement can be made to the segmentation. Part of the 3D data has already been used to correct the focus of objects marked with GFP. The part of the 3D data not used for this method is the mean of  $G(z)$ , the vertical intensity distribution (or equivalently the

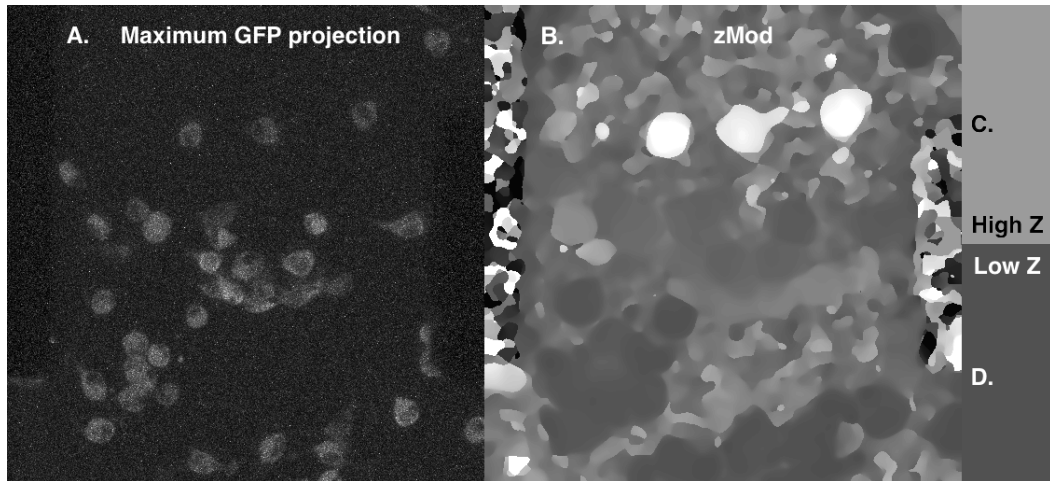


Fig. 4.3 This is an example of the zMod result. The value of each pixel in the image is proportional to the Z value of the maximum intensity of the GFP profile. This is a rough indicator of the level of the object at this XY, but not necessarily every part of the object. In B, continuous patches of similar level correspond to cells marked with GFP. This is the second most useful result of this study as it allows information from the GFP to help find features in the brightfield.

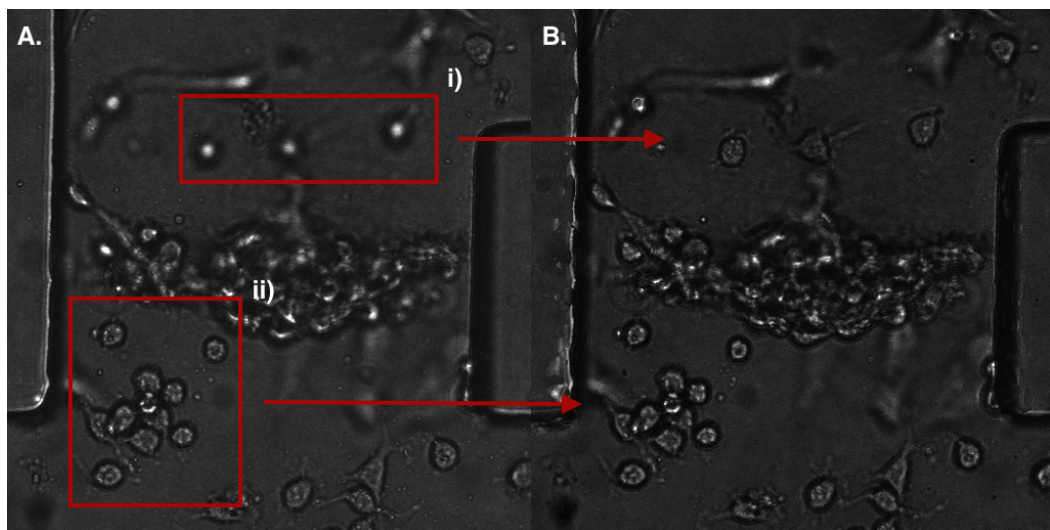


Fig. 4.4 This image, zBF, is the most important outcome of this research. It shows that information from the GFP channel can be used to locate useful edges in the brightfield, that can in turn be used to segment cells and provide accurate numerical properties of the cells over time. It is generated by sampling from the set of brightfield data at a single frame and placing a pixel value into the final zBF image from the level indicated by zMod. In this way, the majority of the data in the brightfield stack is discarded, leaving only the most relevant information to each cell marked with GFP. A shows the original brightfield at a roughly central level ( $Z = 37$ ). The marked regions i) and ii) show two sets of cells at different levels. The cells in set i) are blurred in A since they do not lie close to  $Z = 37$ . The red arrows point from these groups to the corresponding cells in the zBF image, B. Note that both sets are now in focus despite their original level difference.

variance due to the linear relationship). This can indicate presence of an object more reliably than the absolute value of the GFP. Pixels with very different values in the GFP can have similar values in the mean image since the profiles are normalised such that only the shape of the distribution matters. If the mean of the normalised and inverted (since low mean/high variance indicates an object) GFP profile for each pixel in a frame is found, a new image, "zVar" can be made. Depending on the linear smoothing of the original data (the parameter  $R$ ), the boundary of objects in the mean image can extend beyond the edges of objects in the brightfield. This is a limitation of the method, but it can be used to impose a maximum boundary on the extent of the object. Furthermore, since this image depends not on the absolute intensity of the GFP in different parts of the object, but instead on its variance, it can give a more consistent picture of the cell than the maximum projection of the GFP. Outer regions of the cell such as protrusions tend to have lower absolute amounts of GFP, but a similar variance to the interior of the cell.

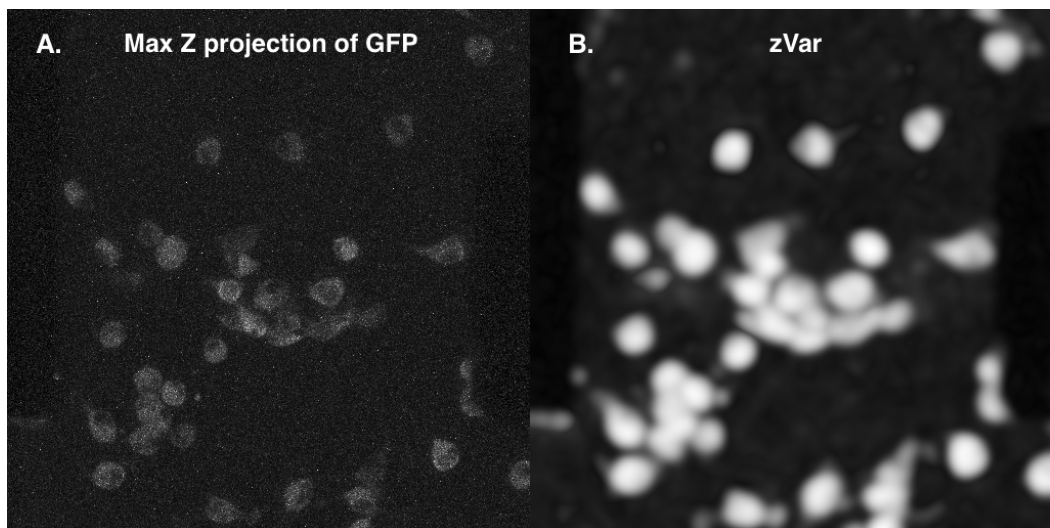


Fig. 4.5 As shown in Figure 4.2, each pixel in XY can be characterised by simple numerical properties such as the mean and variance of the GFP profile. Since, due to normalisation, the mean and variance are linearly dependent, one parameter can be chosen to represent each pixel in XY. If a new image is made with this number used as the value for each pixel, the result is the zVar image. When compared with the maximum Z-projection of the GFP (the maximum value of each column of pixels in Z is used as the representative value for the resulting image, thus the distribution of values in the 3D image is "projected" into 2D), it is clear that the outlines of cells are well represented by zVar. Although the quality of the edges is not an improvement on the GFP, it shows more reliably the full extent of the cell marked by GFP. The GFP fluctuates more in different parts of the cell.

The extra extent of the zVar image is exploited to provide a maximum boundary for segmentation, this is combined with zMod to produce outlines around cells. This does not require the edges to be followed correctly, but only needs to enclose the general shape of

the cell. A further image, "zUnique", can be used to better highlight where the cells edges are. This image takes the intensity of pixels found at a certain level according to zMod, and amplifies them based on their maximum intensity. This is shown in Figure 4.6 These shapes are then segmented to separate objects or even rough groups of objects. The outlines of the segmentation are used to generate artificial edges using a DoF (Difference of Gaussians) edge model. These edges cut through background values that are similar in intensity to the interiors of cells. If there is a gap in the cell edge with an intensity close to the background, the segmentation will expand into the background and cause a major overestimation of the area of the cell. This image is called "zEdge" and is the image for each frame used to provide the final segmentation data for each experiment. An example is shown in Figure 4.7.

The algorithm to produce zUnique is as follows:

1. Find the list of unique Z values in zMod.
2. For each unique Z value, find the pixel at this Z with the maximum intensity.
3. Change every pixel at this Z to this intensity.

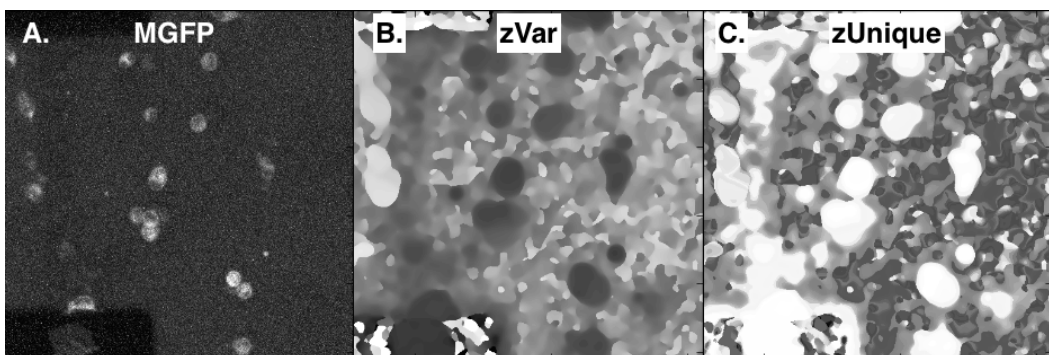


Fig. 4.6 As discussed for Figure 4.5, the inconsistent amounts of the GFP intensity in different parts of the cell is compensated by looking at the variance rather than the absolute intensity. In the same way, continuous areas of similar Z can show the extent of the cell. zUnique amplifies the intensity of pixel in zVar based on the number of pixels in the image that share the same Z, in addition to being high intensity in the variance. The segmentation of this image can provide a maximum boundary for the more precise segmentation of the brightfield and prevent errors such as those shown in Figure 3.6. A shows the Maximum GFP image. B shows the variance image, zVar. C shows the zUnique image. The bright regions in C can be segmented and used to create the zEdge image, shown in Figure 4.7.

## 4.6 Protrusion measurement

One of the main aims of this study is to accurately measure the lengths and orientations of the cell protrusions to gather useful data on cell behaviour. The protrusions were measured

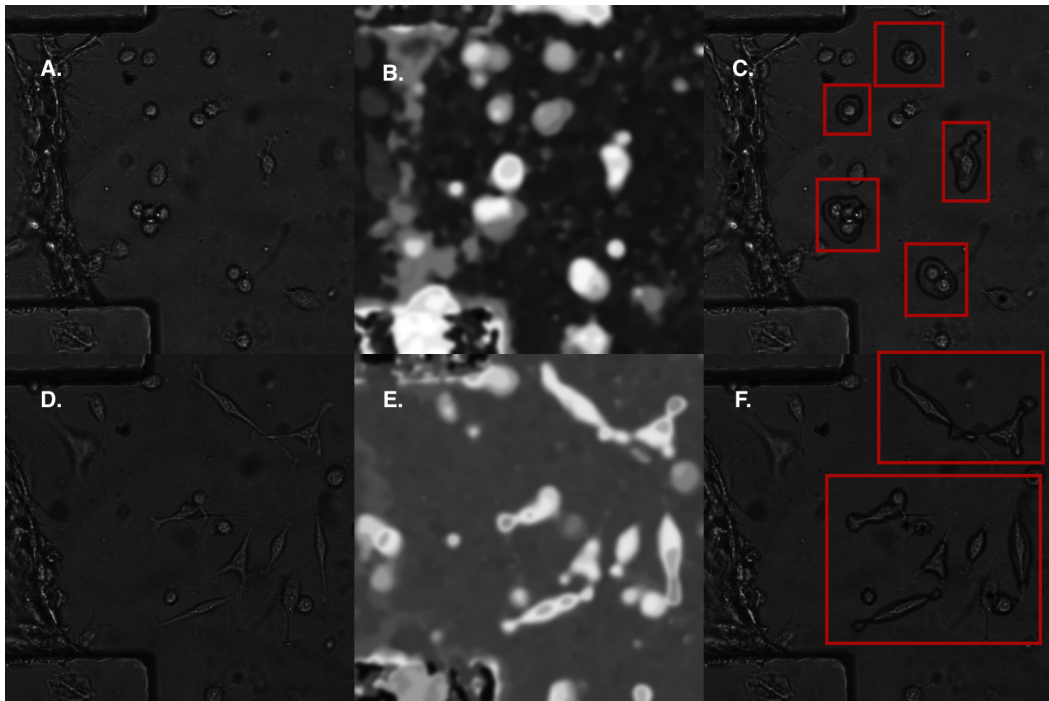


Fig. 4.7 As shown in Figure 3.9, the edges in the brightfield have a particular profile. This profile in Z, and also the profile in XY, can be generalised and used to generate “fake” edges in the image zBF image. This is done by subtracting values from the zBF according to the shape of the edge in XY. These artificial edges follow the edges of the zUnique image. This will then prevent a large amount of segmentation errors. Images A and D are two different frames from a single experiment. B and E show the zVar images from these frames and C and F show the zEdge image generated by superimposing the edges from the segmentation of B,E onto A,D. The red outlines in C,F show the dark artificial edges surrounding the cells. These outlines are from the segmentation of the zUnique images.

by plotting the outline of the cell on a polar graph and measuring the divergence from a smooth circular shape as measured from the calculated cell centre. This is shown in Figure [fig]. The protrusions show as peaks in this plot and their length is measured from the tip of the peak to the mean radius, not the centre of the cell. An example of a protrusion that can be measured is shown in Figure 4.8.

## 4.7 Summary of the method

To summarise the steps taken to pre-process 3D image data for segmentation:

1. Smooth the 3D GFP data to reduce noise. This can be from scattering, reflection or optical properties of different materials in the experiment.

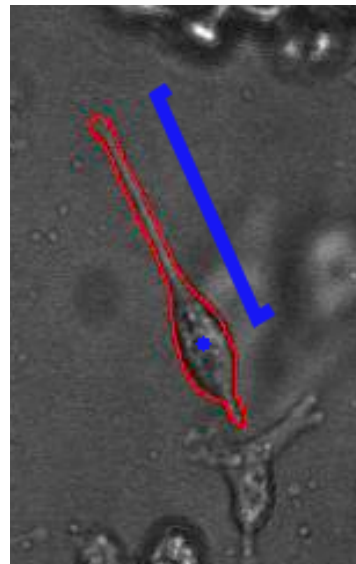


Fig. 4.8 In this study, the length of the protrusion is defined from the centre of the cell. This centre can be the manually marked point or the calculated centre of the cell mask after recognition. Both have their disadvantages. A manually chosen point might lie away from the true nucleus due to human error, but an automatically chosen point could be placed in an extension of the cell depending on the algorithm used.

2. For each pixel in XY for the 3D data, find the vertical intensity distribution in Z, or "profile", for each pixel and evaluate its properties.
3. Using the profile for each XY position, create an image where the value of a pixel is proportional to the Z level at which the maximum intensity of GFP occurs. This is zMod.
4. For zMod, there are three parameters that must be chosen:  $R$ , the radius of the linear smoothing kernel, which affects only the GFP in XY;  $\Delta Z$ , the vertical shift to locate the ideal edges for segmentation; and  $\Sigma$ , the size of the gaussian smoothing kernel, which affects the GFP in Z.
5. Map the Z values in zMod to the stack of image data for the brightfield. Select pixel values from the brightfield whose Z level corresponds to that indicated by zMod and place them into a new image, called zBF.
6. Although zBF now contains in-focus representations of each object marked with GFP, a further improvement can be made using the outlines of the GFP variance image. The variance image, zVar, takes the variance of the normalised GFP profile as the value of each pixel.

7. zVar and zMod can be used to make zUnique by finding maximum GFP values for each unique Z to more consistently highlight cells. This gives a maximum extent of the cell and limits segmentation to a boundary to prevent it from extending into the background and incorrectly judging the area of a cell.
8. The final image, zEdge, is prepared for segmentation by using the zVar and edges of regions in zMod to automatically draw edges on the image that follow a similar edge profile to the dark edges found in the zBF image. zEdge then contains the same information as zBF, but with bounding edges beyond which the segmentation cannot extend.
9. Finally, once segmentation is complete, cell properties such as project area can be obtained along with protrusion lengths and orientations. Protrusions are found by radially plotting the distance of the edge from the centre point and designating outliers as protrusions.

Figure 4.9 below shows the full paradigm of the method.

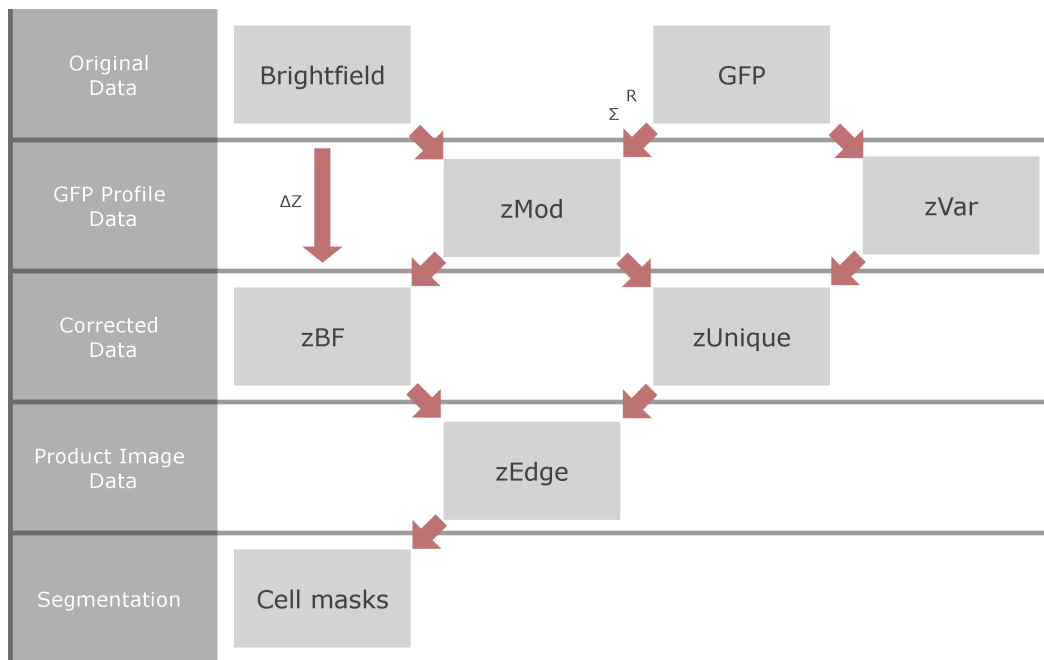


Fig. 4.9 This flow chart shows the full method from the original data to the final product images and the segmentation data. The first level shows the original data, brightfield and GFP images. They are combined along the arrows to yield products with varying uses until the final zEdge image and the segmentation are produced. Parameters used ( $R$ ,  $\Delta Z$ , and  $\Sigma$ ) are marked on the arrows where they are relevant.



# **Chapter 5**

## **Image processing results and discussion**

### **5.1 Introduction**

To compare this method with previous work, the images generated were evaluated based on their use in segmentation as compared with a manually segmented subset of the data. The methods, Selinummi, Maximum GFP, and the current method, can be compared under similar conditions using the same dataset. A readily available property of the cell instances found is the projected cell area. Other properties are the number and orientation of the cell protrusions. These will also be compared to judge the difference between the methods. An example of the comparison between the original brightfield and the final zBF image can be seen in Figure 5.1.

Despite the improvements made, the method developed is not without error. There are parameters that have optimal ranges, but outside those ranges, the method can fail. Some physical properties of the environment can limit the effectiveness of the method, for example, if the level of the GFP is too low to generate an accurate estimate of the Z level, the focus of GFP marked objects will not be corrected accurately, and the results will not be useful. Additionally, some configurations of cells in close proximity can cause problems for this method. A clear example is when two cell lie vertically one on top of the other, causing two visible peaks in the GFP. This, and other examples are discussed in Chapter 4.

A common problem when comparing methods of the segmentation is that there is no objective “ground truth”, or definitely correct answer to the question of the shape parameters of the objects of interest. In their paper, Selinummi et al. attempted to define the ground truth as the segmented shape from the GFP projection [12]. This method is a poor representation of the cell and is prone to errors. For this reason, the ground truth chosen for the comparison of the methods shown here is the manual segmentation, or outlines of the cells drawn by eye on the zBF image. Only of sample of the frames are considered since manual segmentation

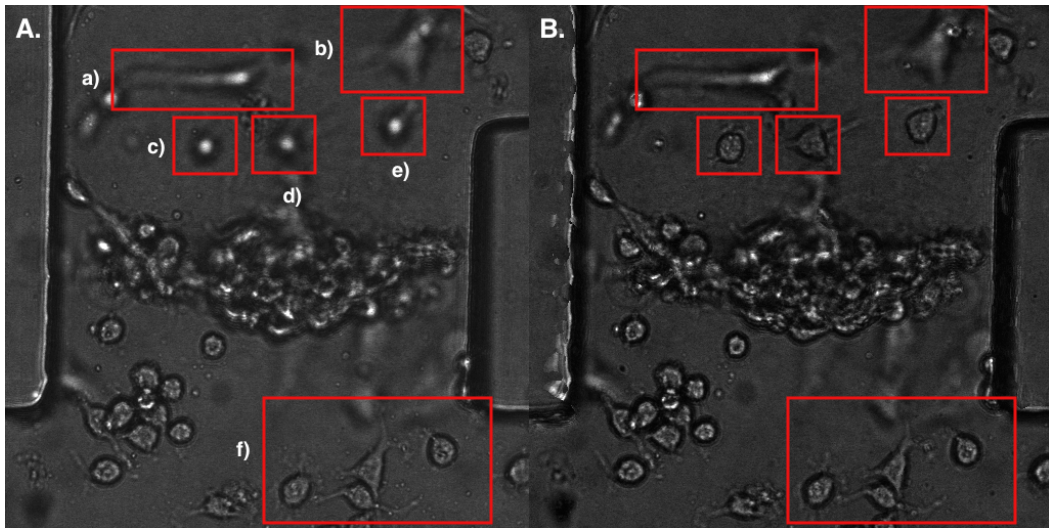


Fig. 5.1 This is a side-by-side comparison of the zBF modification with a single slice of the original brightfield data. The changes that have been made are mostly the adjustment of focus in the appearance of cells that are marked with GFP. Note first of all that cells a) and b) have not been adjusted. These are not marked with GFP and are not affected by any of the algorithms. Cells c), d), and e) originally appear to be out of focus in image A, but in B, they appear in focus. This is part of the correction made. The cells in group f) have been adjusted, but their corrections lie much closer to the focus they originally occupied in this slice. They still appear in focus. All cells marked with GFP have been level corrected. This is the most powerful result of this study.

is very time consuming. Yet another problem, is that not even the manual segmentation can be considered the ground truth. The human eye cannot be trusted to determine the shape of an object which it is totally unfit to identify in an environment that does not lend itself to casual observation. Despite this obstructing piece of philosophy, the final judgement must lie with something, and the best thing available is human vision, which is not saying much in the microscopic world. We are left with no choice but to accept a system of pattern recognition whose highest recommendation is that it insists on discovering human faces wherever it looks [4].

## 5.2 Parameter sensitivity study: $R$ , $\Delta Z$ , $\Sigma$

The three parameters that contribute to the generation of zBF must be carefully chosen, since a low quality result will be useless for segmentation. An analysis of the sensitivity of the result to changes in the parameters can be used to determine the optimum values. Below, some examples of parameters chosen outside the optimal ranges are shown and some consequences of their segmentation is investigated.

### 5.2.1 The radius of GFP linear smoothing: $R$

The parameter  $R$  is the radius of the linear smoothing filter applied to the GFP in order to generate a profile for a point in XY. The filter mixes values in XY, but not Z. It has the effect of reducing noise and making transitions between levels of neighbouring pixels more fluid. This helps to reduce the problem of cross-level artifacts, discussed in Section 5.5. In the case where neighbouring objects in XY have very different levels in Z, the level transition would be smoothed such that the point half way between them would be assigned to a level half way in Z. While this case has not been observed, it could lead to strange results, such as half of each cell being in focus, while the halves closest to the other cell are out of focus. This would depend on the radius of the linear filter, but at a certain point, the information is too smoothed and ceases to be useful. Below in Figure 5.2 is an example of the linear filter set too high. The logical limit is a smoothing filter the size of the image itself in XY. This would simply yield the sum or mean of the GFP for each focal plane, which would not provide any more information than where most of the cells were found in the environment.

On the other hand, if the size of the linear filter is too low, such as a single pixel, the noise in the GFP would dominate the Z estimate, leading to highly fluctuating Z values across even a single cell. The result in the zBF image is an extremely noisy cell interior and edge, surrounded by an equally noisy background. This does not lend itself to accurate segmentation. Figure 5.2 is an example of the linear filter using a small  $R$ .

### 5.2.2 The brightfield level correction: $\Delta Z$

The weakest part of the method is the spatial relationship between the brightfield and the GFP and the decision about the value of  $\Delta Z$ . The brightfield is subject to fluctuations from the autofocus and has no intrinsic spatial information. The most important piece of information relating the GFP and the brightfield is for a hypothetical fixed object in focus in the brightfield, the GFP representation will always correspond to that level of focus. This is because the position of the microscope hardware is constant for a single frame and is set by the autofocus estimate from the brightfield. Assuming the same physical space is represented in both, the GFP can be used to account for the autofocus fluctuations, but the relationship between the GFP representation and the appearance of an object in the brightfield is arbitrary. A cell may be "in focus" as far as possible, but still not be clearly visible by a human. This hinders manual tracking. optimum features for observation may not correspond to optimum features for segmentation. For tracking, it is most effective to observe an object in a solid colour with or without clear edges since the precise shape is not necessary to indicate object centres. For segmentation, a clear object boundary with dark edges and a smooth, uniformly coloured

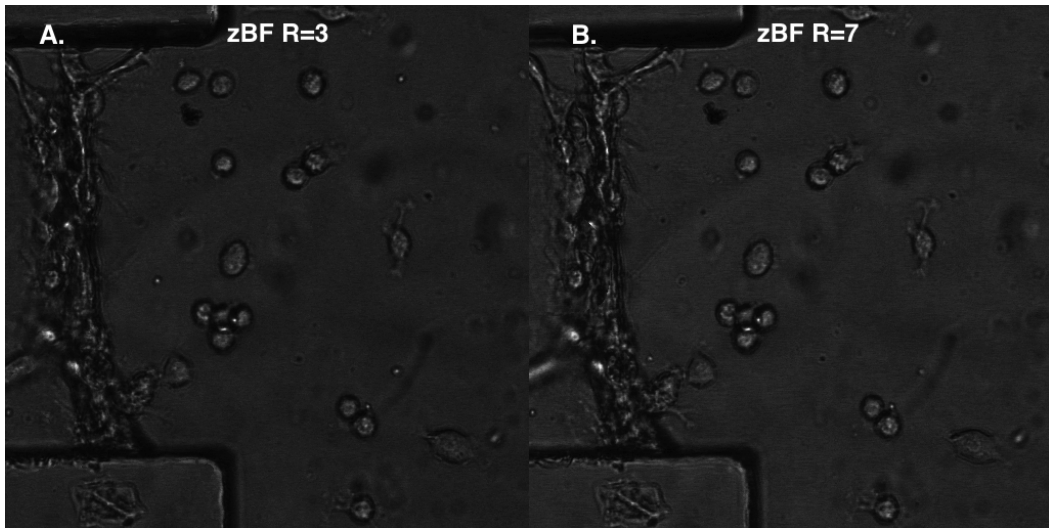


Fig. 5.2 This is an example of the variation of the parameter  $R$ , or the linear smoothing kernel that operates in 2D in the GFP. A shows the zBF image with  $R = 3$ . B shows  $R = 7$ . Note no brightfield information has been smoothed. Brightfield information is accepted or rejected by decisions made using the GFP. Consequently, the parameter  $R$  does not have much of an effect on the zBF image. It can be set to a constant value. That is neither 0, such that noise is not preserved, nor proportional to the size of the image, such that information about features is not destroyed. If the Gaussian kernel were set to the size of the image, this would be equivalent to setting the value of each pixel in the zBF image to the value of the brightfield pixel at the mean  $Z$  at which GFP is found.

interior yields the most accurate shape. This discrepancy is represented by the empirically determined value,  $\Delta Z$ . Changing this value results in what would normally be seen as focussing a simple lens looking at a 2D environment. This effect can be seen in Figure 5.3. Through further study, a value could be found automatically, but the focus level for optimum human observation is highly subjective.

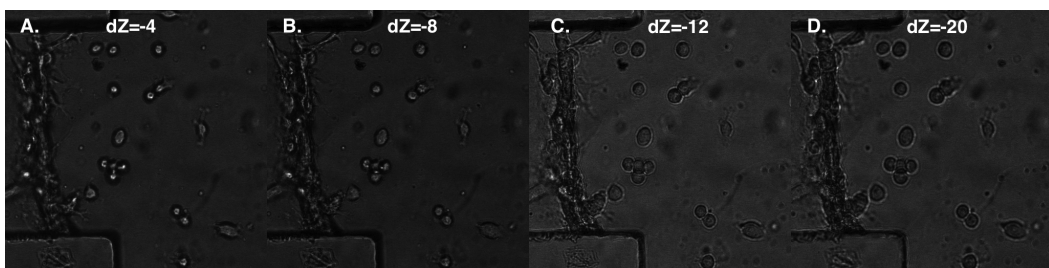


Fig. 5.3 The value of  $\Delta Z$  is very important to the final appearance of the zBF image, shown in A, B, C, D, but must be determined empirically, or by a trusted, previously determined algorithm. It is the level offset between the location of the GFP representations of cells and their brightfield counterparts. Changing  $\Delta Z$  is equivalent to focussing a microscope objective that is looking at a 2D slide or other simple environment. Focussing too far in one direction will have the effect of leaving every corrected object in the environment out of focus.

### 5.2.3 The radius of level Gaussian blur: $\Sigma$

The radius of the Gaussian blur between levels, or  $\Sigma$ , affects how smooth the transitions between levels are in the GFP. It mixes data from different parts of the environment in 3D. This does not affect the output in the brightfield greatly, but it can prevent errors. An example of the variation can be seen in Figure 5.4, and the results of the ignoring this parameter can be seen in Figure 5.13.

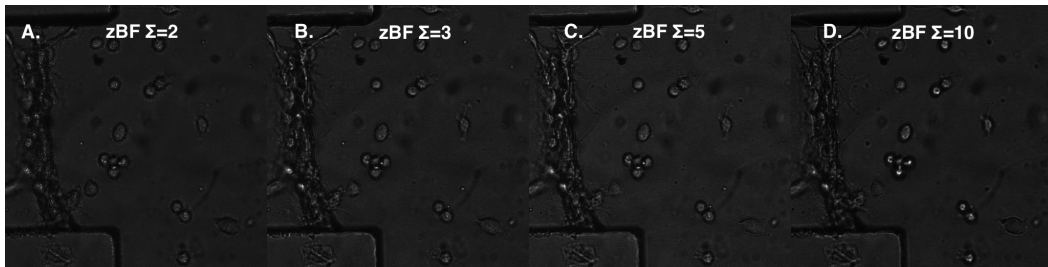


Fig. 5.4  $\Sigma$  is a very important parameter that affects the smoothing of the GFP in 3D. If it is set too high, features can be destroyed very easily. A reasonable value can prevent noise dominating the level corrections. The best example of dominant noise is the image in A. Even though the brightfield is not affected by the GFP processing, the noise in the GFP leads to a very noisy appearance in the values chosen from the brightfield.

### 5.2.4 Final choice of parameters

The three variables used to produce zBF were fixed to the following values. These were also chosen for their effects on zUnique and zEdge:

Parameter	Description	Chosen range	Reason
$R$	Radius of 2D linear smoothing kernel in XY	3-5 pixels	Reduce noise in GFP images.
$\Delta z$	Difference between observed in-focus level and optimal edges for segmentation	-6 to -8 levels	Determined by observation and segmentation testing.
$\Sigma$	Radius of 3D Gaussian smoothing kernel	5-7 pixels	Make transitions between regions with similar Z more gradual to prevent cross-level artefacts. See Figure 5.13.

### 5.2.5 The subject of the background

It should be noted that background pixels in XY that contain very little GFP at any Z, and thus have very flat profiles, are still assigned a value for the Z position. This may appear misleading, as it can be highly random as the “maximum” of a flat distribution is given by the noise alone. This can be seen clearly in the PDMS pillars in Figure 5.5, indicated by an arrow. While this might be thought to produce errors, other means of filtering background can be used that do not rely on the Z position, such as the mean image. It is more reliable to be unbiased when generating the zMod image since there is no certain way of determining whether a particular Z value should be assigned. If filtering must be done eventually, it can be done using other 3D data.

### 5.2.6 Subsequent effects on zUnique and zEdge

The three parameters discussed here can also affect the zUnique and zEdge images in specific ways. Zunique is based solely on the GFP information, so cannot be affected by  $\Delta Z$ , but  $\Sigma$  and  $R$  will affect the smoothing of the zUnique information. Smoothing the GFP will spread the information and the Z placement of the maximum intensity in neighbouring pixels. This could cause the mask of the segmentation of the zUnique image to appear larger with larger  $R$  and  $\Sigma$ . This, in turn, will affect the edges placed into the zEdge image. The edges could become thicker and further away from the mask of the cell. This could allow parts of the background surrounding the cell to be included in the final mask. The zBF component of the zEdge image will be affected by the parameters in the same way as the original zBF image.

## 5.3 zVar and zEdge

The zEdge image uses artificial edges to constrain the segmentation and prevent errors. The artificial dark edges are drawn on the image using the edges from the segmentation of the zUnique channel. The colour profile of the images is determined by scanning the XY brightness profile of in-focus edges in the brightfield. The quality of the edges is determined by the reliability of the segmentation of the zUnique channel, which can lead to errors. Artificial edges can cut off parts of the cell that do not contain enough GFP. An example of this effect is shown in Figure 5.6. If the segmentation fails completely, there will be no edge drawn. In most cases, segmentation of the brightfield in zEdge can continue as normal, although there will be no barrier to stop the segmentation from expanding. This type of effect is shown in Figure 5.7.

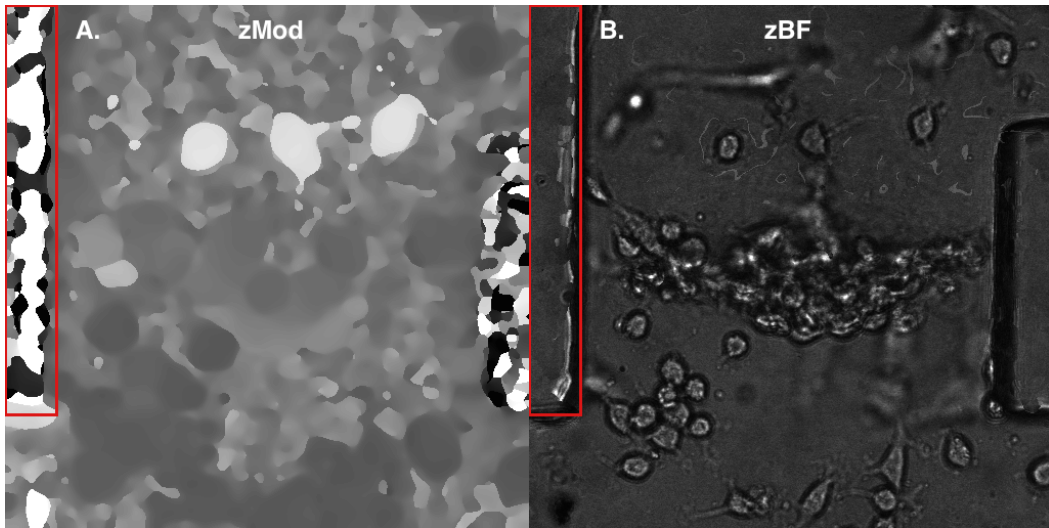


Fig. 5.5 Even the noise and background is assigned a Z value. This seems counterintuitive when applied to the background, but the philosophy of this study is that any analysis or segmentation cannot be biased to sizes and shapes of objects. All locations in an image must be considered and treated equally until enough knowledge has been gathered and assumptions have been made to treat different areas differently. At the zMod stage, there is no certainty or assumptions about the locations or shapes of cells, so all pixels in the image are subject to the same calculations. When a profile is measured in a pixel column that contains no GFP, there will still be background noise and any slight fluctuation will yield a maximum value and its position. This value is placed in the zMod image. The rationale is that it will not affect the segmentation since these areas will be rejected as part of the background anyway. These areas are filtered out at the zVar stage which is dependent on degree of variance. These locations have no variance and will not affect the final result.

## 5.4 Comparison with common methods

Previous methods cannot account for the inconsistencies in the focus fluctuations and so are not really comparable in their quality. Below, some of the results from segmentation of images generated using several different method including the current method. The comparisons here are based on the segmentation area, shown in Figure 5.8 and Figure 5.9, although in reality, judging by the area of segmentation alone is unreliable, and an analysis of all available shape parameters should be done instead. This analysis is partially beyond the scope of this project, but leaves an opportunity for future work. Another method of comparison comes from tracking smaller cell features, such as protrusions, individually. This is also currently beyond the capabilities of the study, but current research can be easily extended to include this. A small example of how protrusions can be tracked and measured is shown in Figure 5.10.

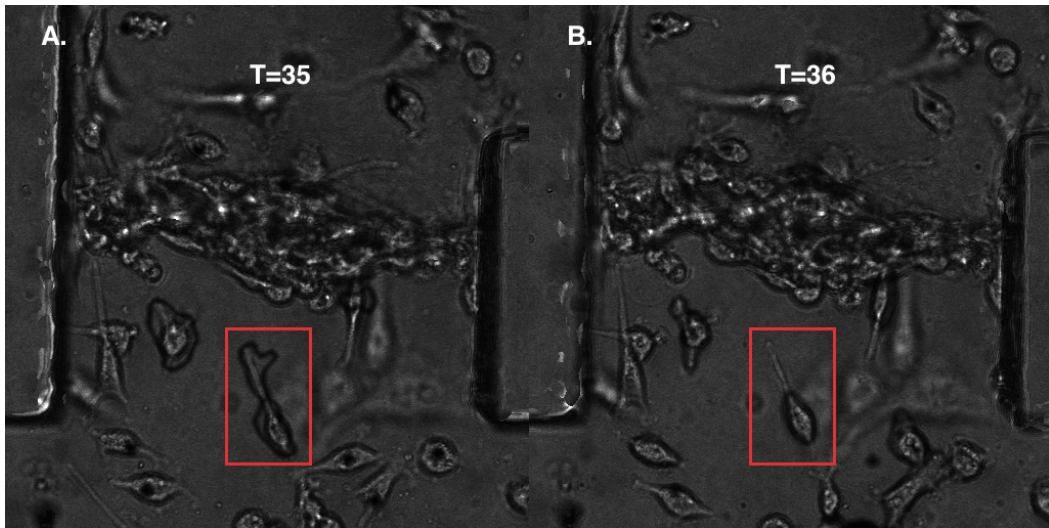


Fig. 5.6 One serious problem with this method is the lack of edge detection in low-contrast regions or frames in the GFP. If, due to a mechanical fault or other variation in the hardware of the microscope, the level of the GFP is lower in one frame, the method will suffer and be unable to level-correct key parts of the cell such as the protrusions. In A, the protrusion has been outlined clearly, but in B, the zEdge image has cut off the protrusion, which will prevent its segmentation. For future work, a compromise can be made between the zEdge segmentation and the unbridled zBF segmentation.

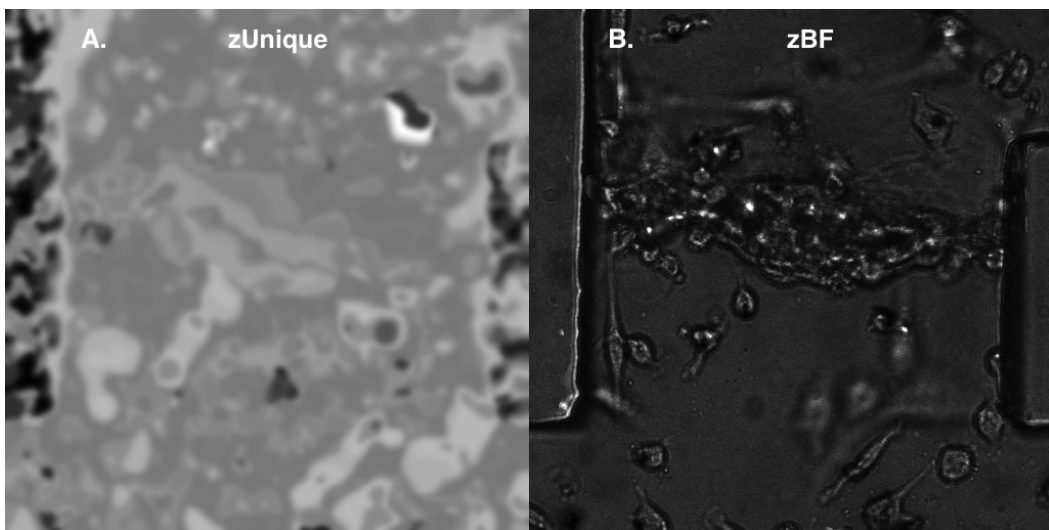


Fig. 5.7 Sometimes, zUnique can yield a low-contrast image, usually, but not necessarily due to low contrast in the GFP. This can prevent the drawing of edges altogether leaving a dark spot at the position of the marker in each cell and possibly negatively affecting segmentation.

## 5.5 Errors and limitations

Several possible errors that would affect segmentation results must be mentioned for completeness. Some of these errors have not been observed, but are possible given certain

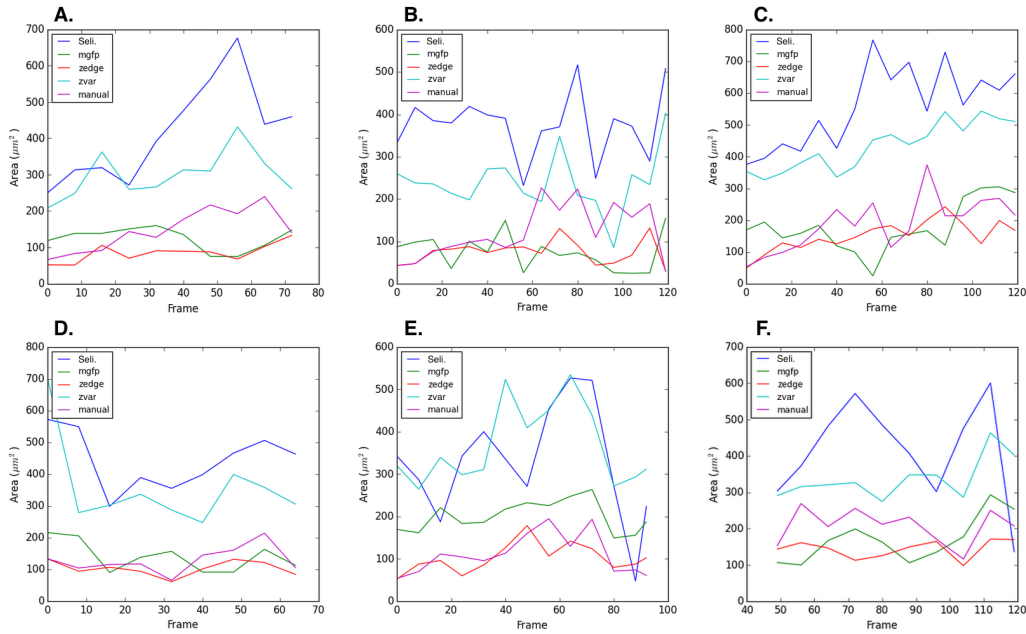


Fig. 5.8 In order to test the method of image modification, the best thing to be done is attempt to segment the images produced. The method of comparison used in the Selinummi paper [12], which involves the comparison with the GFP projection in 3D, is insufficient to be certain about the result of segmentation. For this reason, a sample of the cells were segmented manually to provide a baseline from which to measure. Selinummi refers to this as the “ground truth”. This is shown as the purple line in each plot. The blue line is the method from the Selinummi paper. This suffers from an inability to distinguish between different types of cells and plastic, leading to an overestimate of areas as other material is incorporated into the mask from segmentation.

conditions. Errors can be caused by faults in the microscope hardware, irregularities in the illumination of the environment for any reason, poor choices in imaging setup, or particular configurations of cells that cause the method to fail.

A controversial example of a possible error is a situation where two cells are superimposed in Z. In this case, a GFP profile for a single XY location could have two very prominent peaks. Currently, the method does not attempt to resolve this situation since it has not been observed in the current data, but trivially, it could be resolved by only taking account of the peak with the highest Z level, since the brightfield information is not 3D, and there is no way to recover any edge information about the lower cell if it is obscured. In this case, such a conflict could be noted and the GFP edge, which is not obscured, could act as a fallback for the segmentation. This information would allow the GFP edges, while they are suboptimal, to be incorporated into the outline of the rest of the cell if it is visible elsewhere in the brightfield. To reiterate, this situation has not been observed, but it is theoretically possible in such a 3D environment. A hypothetical example can be seen in Figure 5.11.

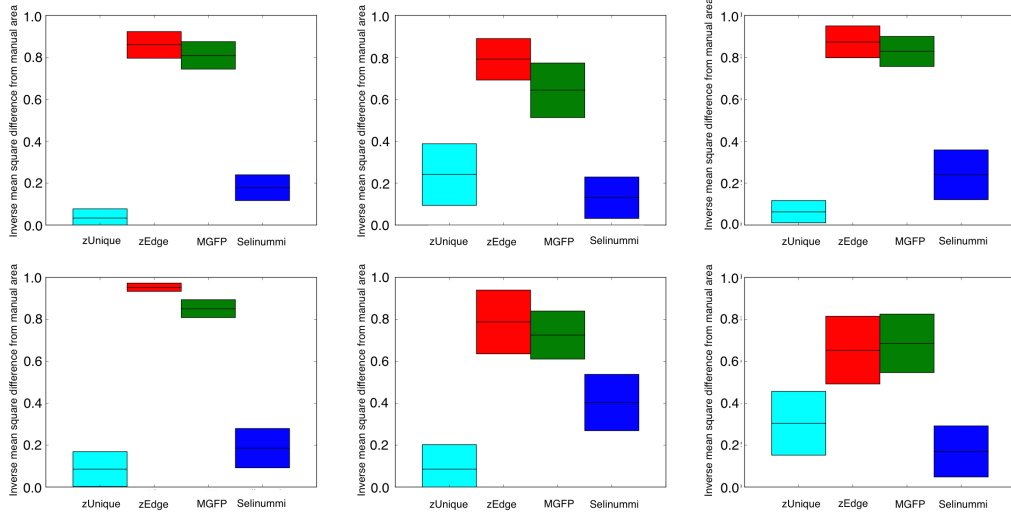


Fig. 5.9 Each plot shows the comparison of the segmented area of different images generated from the original image data. The first two (cyan and red) show the intermediate stage,  $z_{Var}$ , and the final stage of the current processing method,  $z_{Edge}$ . The last two (green and blue) show the maximum projection of the GFP and the Selinummi method respectively. A high score on the y-axis shows a better match to the manually segmented test data. The boxes show the mean (central black line) and variance (coloured box) of time series data for each cell mask. The mean and variance values for a single channel are generated by comparing the area of each mask per frame to the manually drawn mask. This series of differences is then normalised to the maximum difference from all channels at each frame. The mean of this normalised series is found for each channel and inverted, such that a high value represents a typically low difference compared with other channels. Mathematically, this can be expressed as  $v(c) = 1 - \frac{1}{F} \frac{A_f(c)}{\max A_f(c)}$ . Where  $v(c)$  is the final comparison value shown,  $c$  is the channel index,  $F$  is the number of frames,  $f$  is the frame index, and  $A_f(c)$  is the area of the mask for channel  $c$  at frame  $f$ . A similar comparison between the segmentation of the areas can be seen in Figure 5.10.

In some cases, through a hardware fault or a temporary shift in the illumination of the environment, the level of the GFP intensity can drop in the whole experiment. This happened in one experiment done and caused the method to fail in a single frame, and subsequently rendered the area estimates in that frame for all objects unreliable. This effect can be seen in Figure 5.12.

If the illumination of the environment is not uniform, and regions at the top are significantly brighter than the bottom for example, when brightfield pixel values from different Z levels are brought together to generate  $z_{BF}$ , it is possible that the intensities are so different as to be discontinuous, leading to the appearance of a false edge. This type of effect is shown in Figure 5.13. This can be alleviated partially by the choice of  $R$  or  $\Sigma$ , since both control to a certain extent the smoothing between levels. If transitions between levels are smoother, artefacts such as these are less likely to form.

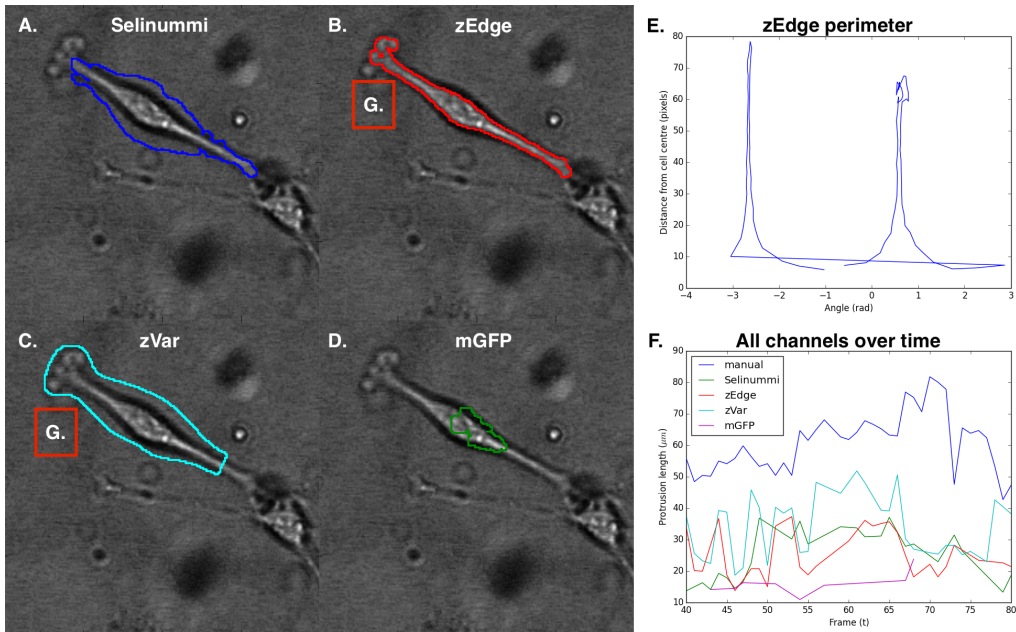


Fig. 5.10 Cell masks can also be compared by how well the extremities of the cell are segmented. ABCD show four different masks of the same cell from four different channels (Selenummi, zEdge, zVar, and mGFP (the maximum GFP projection) respectively). By tracing a line around the perimeter of the shape, a distribution similar to that shown in E can be found for each cell; an ordered list of distance against angle around the centre point. This can then be used to find any peaks that diverge from the mean radius. These can be classed as protrusions and their lengths and orientations found. F shows protrusion length over time for several channels including manually for comparison. Such a comparison is hard to compress into one or two values such as in Figure 5.9. For example, the protrusion on the left, marked G, is longer in the zVar (C) channel than in the zEdge (B) channel, but the zEdge segmentation of the protrusion is closer to the overall shape. Most protrusion lengths will fall short of the true length as segmented manually. This type of analysis is not current quantifiable, but it can be investigated using this method of image pre-processing.

Finally, if the configuration of the microscope is chosen before imaging to yield generally low contrast brightfield images, edges may not be visible in any focal plane. In this case, the method of finding the in-focus representations of cells may not be very useful as no more information is revealed. In this case, an alternative might be to use the segmentation of the GFP primarily and gather what results are available from the brightfield. As with hypothetical superimposed cells, edges from GFP and brightfield channels could be combined, but here it might be more effective to weight the edges found in GFP to be more reliable than those in the brightfield. This is subject for future work.

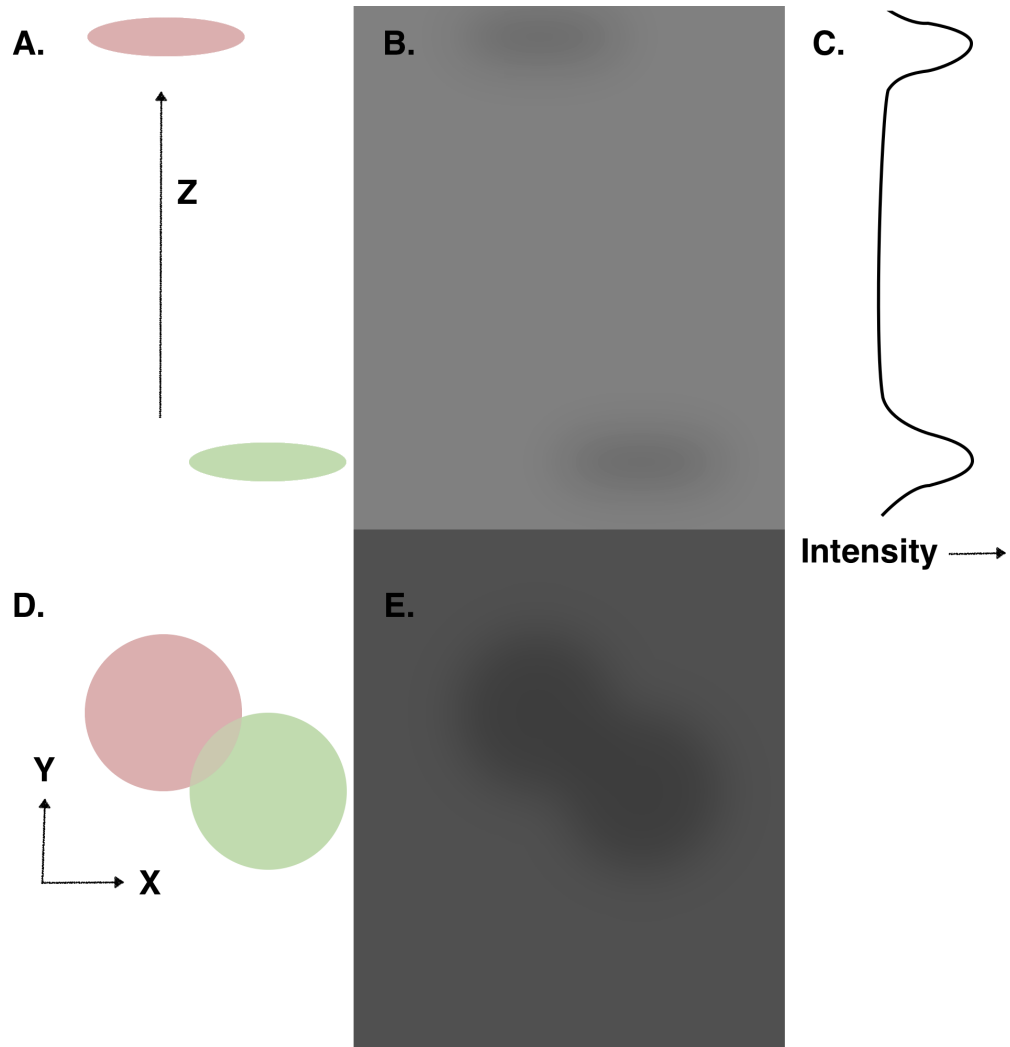


Fig. 5.11 A potential weakness of this method is a situation which has not been fully encountered. If two cells lie superimposed at very different levels in the environment, as depicted in A, it is possible that there will be two distinct peaks in Z as shown in C. In this situation, the current algorithm would take the maximum peak as the value to be added to zMod. If the cell with the greater value is the lower one, the brightfield representation would not be complete. The brightfield information between different levels is mixed and can only be seen from above. The cell above would be the most useful candidate to level-correct. This situation has not been encountered in the current data, and the method would have to be modified to account for this possibility.

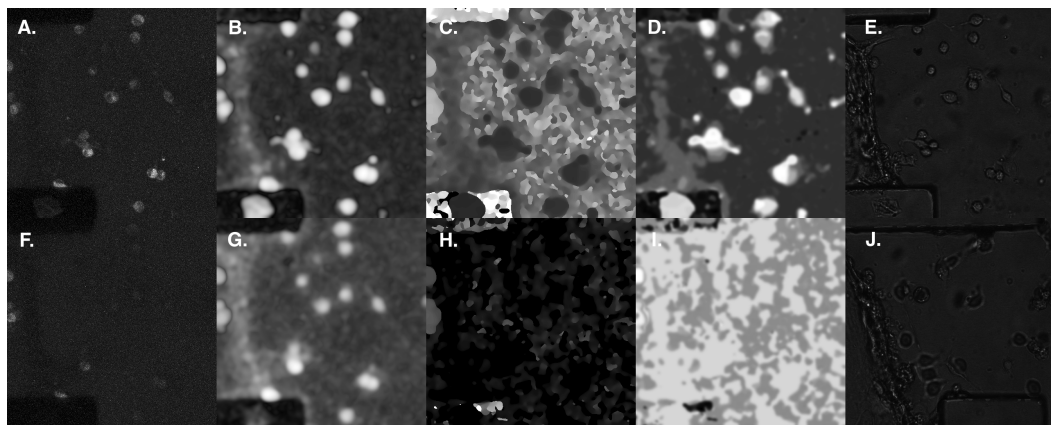


Fig. 5.12 As stated before in Figure 5.6, this method does not work in low GFP conditions. From left to right, the images are A, The GFP Z projection; B, the zVar image; C, the zMod image; D, the zUnique image; and E, the zBF image. ABCDE shows the method under normal GFP conditions. FGHIJ shows the environment one frame later when the illumination has dropped significantly. Note particularly A compared to F. There is very little GFP present. In contrast, the variance image, zVar, still shows a strong response, a testament to the utility of this information. zMod suffers from the drop in GFP lacking a consistent Z location within cells. Similarly, the zUnique contrast drops. The result is an incorrectly level-corrected image in zBF.

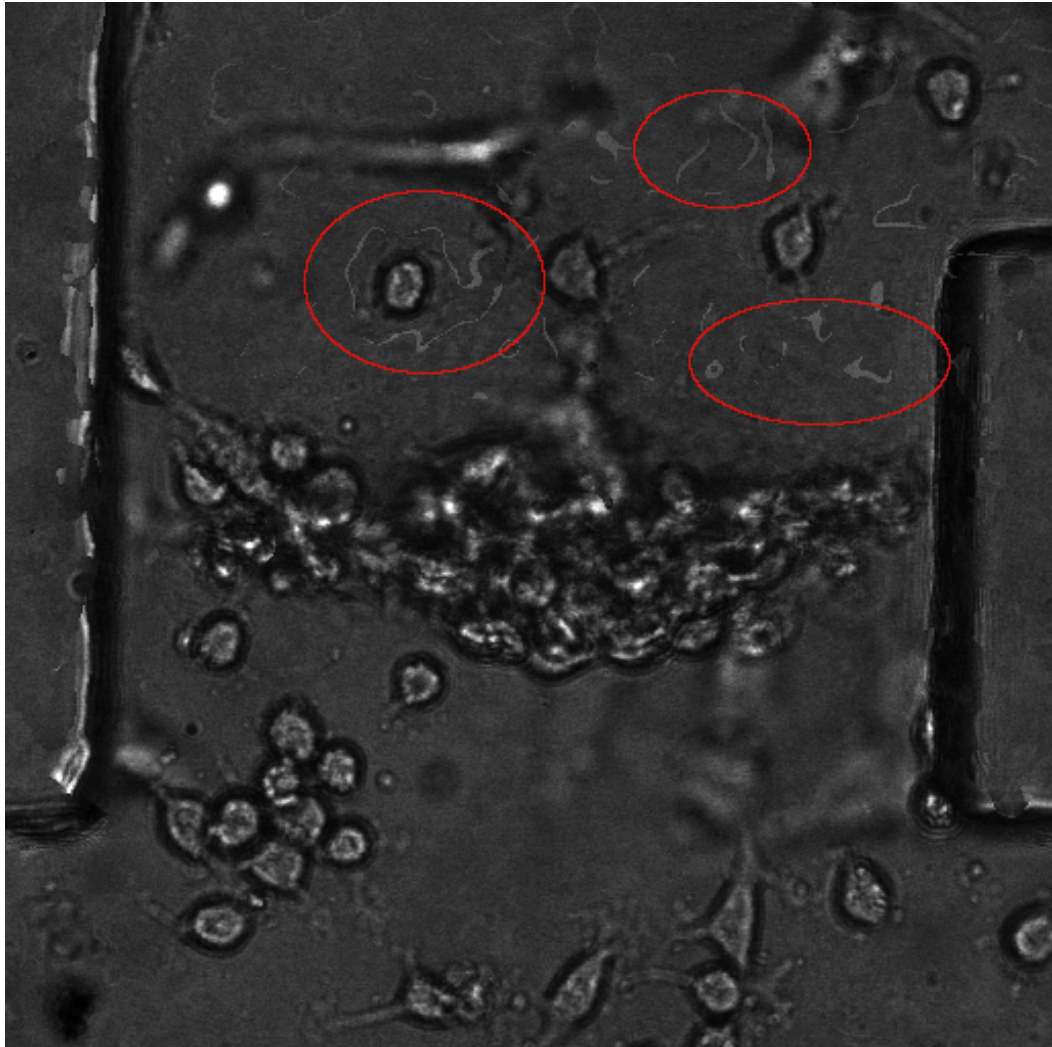


Fig. 5.13 zBF is created by taking brightfield values from all different parts of the image stack. It is possible that illumination at the top and bottom of the stack may differ, sometimes significantly. In this case, darker pixels may be placed in the zBF image adjacent to light pixels from another level. This results in a mottled appearance of the zBF image. The highlighted boxes contain features that could be interpreted as objects or parts of objects by a recogniser. This is possibly a weakness. Improved smoothing methods and gradual object recognition could solve this problem. This means segmentation carried out at each stage of the image modification process could be combined to decrease error at the final stage.

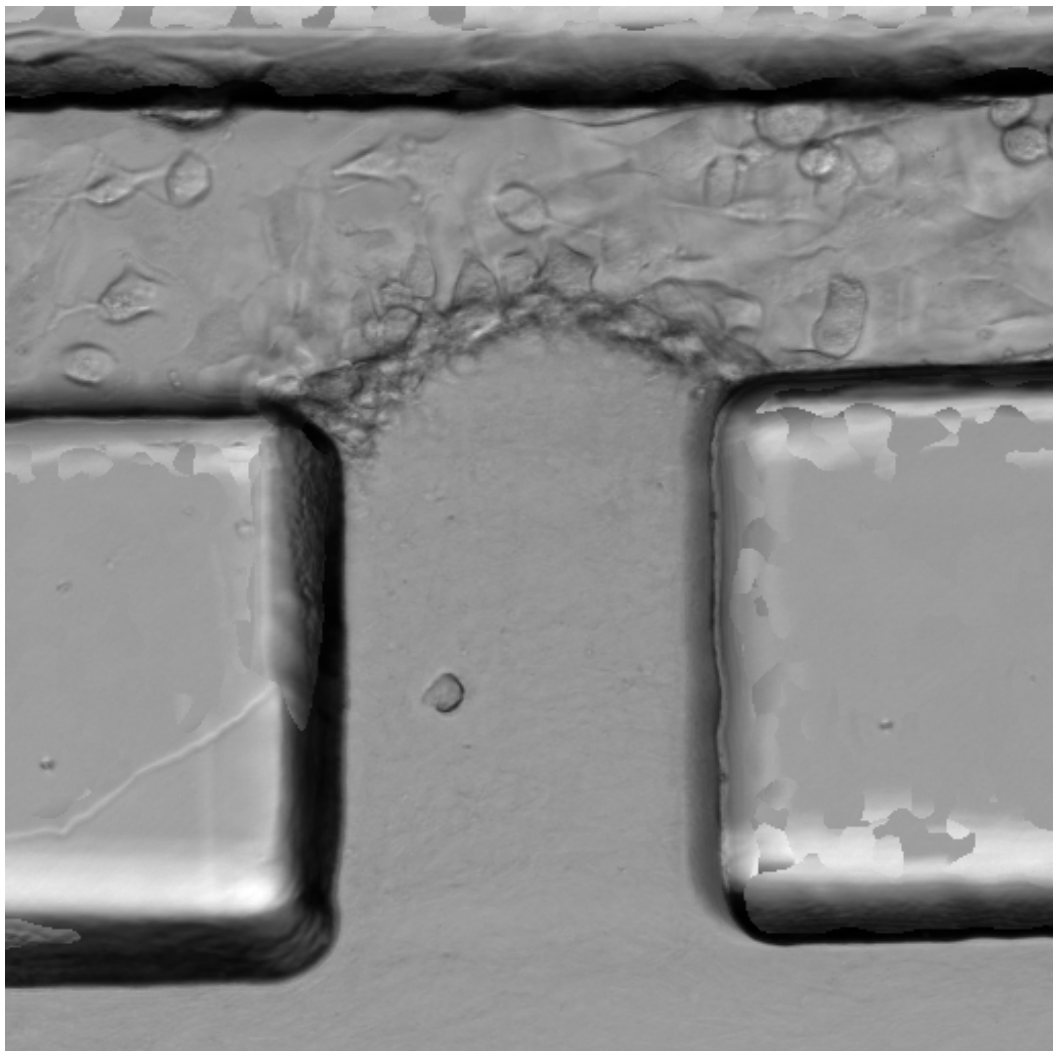


Fig. 5.14 Low GFP intensity is very harmful to this method, but even if the GFP is very high contrast with low noise, a lack of brightfield contrast can also prevent the method from working. If the brightfield has low contrast, then edges of cells and other objects will not be as visible. Even if the images are level corrected properly, there might not be enough information to segment the cells properly. Shown is an example of an experiment with very poor contrast in the brightfield. This cannot be solved numerically and must be carefully adjusted in the microscope prior to imaging.



# **Chapter 6**

## **Conclusion**

### **6.1 Summary**

Given the limitations on cell segmentation in 3D image data, the method described in this study performs well in overcoming problems and improves on the previously proposed method by Selinummi et al. by a large margin. It also compares favourably with previous attempts at segmentation using conventional means, such as Z projection of the GFP and segmentation at a constant Z level. It can also be used as a method to correct the autofocus fluctuations in brightfield data, which while not originally intended, is a natural consequence of the treatment of the 3D data.

The method depends on several parameters, such as R, the radius of the linear smoothing kernel;  $\Delta Z$ , the level correction of the edges; and  $\Sigma$ , the size of the gaussian smoothing in 3D. The method is mostly invariant under these parameters, but can be adjusted using  $\Delta Z$  depending on the type of edges needed for segmentation. Ideally, these parameters would not have been chosen, they would simply be used to explore the data available. In this method, a lot of data is discarded, leaving the level-corrected images.

Throughout this study, the guiding philosophy has been that a cell segmentation method cannot be fully automatic, and must rely on human input as long as cells cannot be modelled as part of the segmentation. For now, the human brain is the most consistent pattern recognition available, but future methods could allow for more complex segmentation, such as matching mechanical models of cells to corresponding images and calculating the most likely routes for a cell to take. This philosophy has led to the creation of different images, such as zVar, which, while useful for segmentation, are most useful for observation and for letting a human know where to look for cells and allow for easier cell tracking.

## 6.2 Further work

This research leaves many opportunities for future study, such as improved cell segmentation and tracking, with and without human aid. This study has focussed only on the pre-processing of 3D image data to improve segmentation of cells in a 3D environment. Despite advances made, the process still does not use 3D information to help any segmentation algorithm. The segmentation is completely outsourced to systems like Cell Profiler and ImageJ. The current research also does not make any assumptions about sizes or shapes of cells, their features, or their behaviour or movements. Narrowing the search space by making assumptions or modelling the cells and their movements could result in more accurate segmentation. Below are some examples of expansion from this work.

### 6.2.1 Enhanced microscope imaging with live cell tracking

Throughout the current dataset, the images capture a wide area to encompass the movements of many cells and their interactions with the environment. This is done to make any measurements more relevant to the entire experiment, without focussing on one or two cells only. The problem with this approach is the large amount of empty space in the image that is processed due to lack of information about objects of interest. Each pixel of the image takes time to measure and process. Most parts of the image contain no objects and their imaging is not relevant to the experiment. Using this method of locating cell edges in 3D, a more accurate estimate of the portion of the image occupied by cells could be found and used to constrain the search space of the microscope. The field of view could be made to shift dynamically during the imaging period. This would result in shorter lengths of time between frames and the ability to zoom in on particular cells, raising the XY resolution available. This could be done by modifying microscope software to use this method on the fly.

### 6.2.2 Pre-processing to segmentation

The current method was designed to pre-process images to be passed to segmentation software. Instead of pre-processing the images, the information could be used to directly segment the images. There is no current segmentation method that investigates the vertical distribution of the brightfield data in 3D without compressing it, such as the Selinummi method. This is an open area of study and could be added to easily following on from the current research. This would also allow an analysis of shape parameters given a whole new dimension of data. Protrusion characteristics and finer details of cell movement could be

recorded using this extra data. This would allow for more accurate cell tracking by adding to the information about cells as they change and move.

### 6.2.3 Cell dynamic modelling

During segmentation, assumptions are made about the size and shape of a cell and the properties of its surroundings in order to narrow the search space that must be analysed. These assumptions include types of edges and colour profiles inside cells; textures and known structures such as a nucleus or protrusions. The more specific the assumptions about a cell, the more constrained the search space becomes, but also the more biased any recogniser becomes. If assumptions are made with very little information, such as “We are looking for cells with a radius of approximately 10 microns”, the recognition will be biased towards circular structures with sizes around 10 microns, even structures which, upon further inspection, are not cells. Adding information allows better assumptions to be made. If the cells could be modelled using the information found in 3D using this method, the movements of each individual cell could be better understood allowing assumptions about their shape to be refined. Making assumptions about cells individually rather than all cells as a whole could lead to far more powerful segmentation.



# References

- [1] Canny, J. (1986). A computational approach to edge detection. *IEEE Transactions on Pattern Analysis and Machine Intelligence*, PAMI-8(6):679–698.
- [2] Carlsson, K., Danielsson, P. E., Liljeborg, A., Majlöf, L., Lenz, R., and Åslund, N. (1985). Three-dimensional microscopy using a confocal laser scanning microscope. *Opt. Lett.*, 10(2):53–55.
- [3] Firestone, L., Cook, K., Culp, K., Talsania, N., and Preston, K. (1991). Comparison of autofocus methods for automated microscopy. *Cytometry*, 12(3):195–206.
- [4] FYFE, S., WILLIAMS, C., MASON, O., and PICKUP, G. (2008). Apophenia, theory of mind and schizotypy: Perceiving meaning and intentionality in randomness. *Cortex*, 44(10):1316–1325.
- [5] Halldorsson, S., Lucumi, E., Gómez-Sjöberg, R., and Fleming, R. M. (2015). Advantages and challenges of microfluidic cell culture in polydimethylsiloxane devices. *Biosensors and Bioelectronics*, 63:218 – 231.
- [6] Herold, K. E. and Rasooly, A. (2009). *Lab-on-a-chip technology*, volume 2, chapter 16, pages 269–284. Caister Academic.
- [7] Parvati, K., Prakasa Rao, B. S., and Mariya Das, M. (2008). Image segmentation using gray-scale morphology and marker-controlled watershed transformation. *Discrete Dynamics in Nature and Society*, 2008:1–8.
- [8] Peters, V. G., Wyman, D. R., Patterson, M. S., and Frank, G. L. (1990). Optical properties of normal and diseased human breast tissues in the visible and near infrared. *Physics in Medicine and Biology*, 35(9):1317.
- [9] Poland, S. P., Wright, A. J., and Girkin, J. M. (2008). Active focus locking in an optically sectioning microscope utilizing a deformable membrane mirror. *Opt. Lett.*, 33(5):419–421.
- [10] Reymond, N., d’Agua, B. B., and Ridley, A. J. (2013). Crossing the endothelial barrier during metastasis. *Nat. Rev. Cancer*, 13(12):858–870.
- [11] Saluja, S., Singh, A. K., and Agrawal, S. (2013). A study of edge-detection methods. *International Journal of Advanced Research in Computer and Communication Engineering*, 2(1):994–999.
- [12] Selinummi, J., Ruusuvuori, P., Podolsky, I., Ozinsky, A., Gold, E., Yli-Harja, O., Aderem, A., and Shmulevich, I. (2009). Bright field microscopy as an alternative to whole cell fluorescence in automated analysis of macrophage images. *PLoS ONE*, 4(10):e7497.

- [13] Stetler-Stevenson, W. G., Aznavoorian, S., and Liotta, L. A. (1993). Tumor cell interactions with the extracellular matrix during invasion and metastasis. *Annu. Rev. Cell Biol.*, 9:541–573.
- [14] Sung Liao, P., sheng Chen, T., and choo Chung, P. (2001). A fast algorithm for multilevel thresholding. *Journal of Information Science and Engineering*, 17:713–727.
- [15] Tibshirani, R. (2011). Regression shrinkage and selection via the lasso: a retrospective. *Journal of the Royal Statistical Society: Series B (Statistical Methodology)*, 73(3):273–282.
- [16] Tsui, J. H., Lee, W., Pun, S. H., Kim, J., and Kim, D. H. (2013). Microfluidics-assisted in vitro drug screening and carrier production. *Adv. Drug Deliv. Rev.*, 65(11-12):1575–1588.
- [17] Wang, H., Li, G., and Tsai, C.-L. (2007). Regression coefficient and autoregressive order shrinkage and selection via the lasso. *Journal of the Royal Statistical Society: Series B (Statistical Methodology)*, 69(1).
- [18] Yan, W. Z. and Deng, D. Z. (2012). Study of image edge detection techniques. *AMR*, 505:393–396.
- [19] Zheng, W., Wang, Z., Zhang, W., and Jiang, X. (2010). A simple pdms-based microfluidic channel design that removes bubbles for long-term on-chip culture of mammalian cells. *Lab Chip*, 10:2906–2910.
- [20] Zou, J., Ye, Y., Welshhans, K., Lurtz, M., Ellis, A. L., Louis, C., Rehder, V., and Yang, J. J. (2005). Expression and optical properties of green fluorescent protein expressed in different cellular environments. *J. Biotechnol.*, 119(4):368–378.